

1 **Methane, carbon dioxide, and nitrous oxide emissions from two**  
2 **clear-water and two turbid-water urban ponds in Brussels (Belgium)**

3 Thomas Bauduin <sup>1,2</sup>, Nathalie Gypens <sup>1</sup>, Alberto V. Borges <sup>2</sup>

4 <sup>1</sup>Ecology of Aquatic Systems, Université Libre de Bruxelles, Belgium

5 <sup>2</sup>Chemical Oceanography Unit, University of Liège, Belgium

6 Correspondence to: Thomas Bauduin ([thomas.bauduin@ulb.be](mailto:thomas.bauduin@ulb.be)) and Alberto V. Borges ([alberto.borges@uliege.be](mailto:alberto.borges@uliege.be))

7 **Abstract.** Shallow ponds can occur either in a clear-water state dominated by macrophytes or a turbid-water state dominated  
8 by phytoplankton, but it is unclear if and how these two alternative states affect the emission to the atmosphere of  
9 greenhouse gases (GHGs) such as carbon dioxide (CO<sub>2</sub>), methane (CH<sub>4</sub>), and nitrous oxide (N<sub>2</sub>O). We measured the  
10 dissolved concentration of CO<sub>2</sub>, CH<sub>4</sub>, and N<sub>2</sub>O from which the diffusive air-water fluxes were computed, in four urban ponds  
11 in the city of Brussels (Belgium): two clear-water macrophyte-dominated ponds (Silex and Tenreuken), and two turbid-water  
12 phytoplankton-dominated ponds (Leybeek and Pêcheries) on 46 occasions over 2.5 years (between June 2021 and December  
13 2023). Ebullitive CH<sub>4</sub> fluxes were measured with bubble traps in the four ponds during deployments in spring, summer, and  
14 fall, totalling 48 days of measurements. Measured ancillary variables included water temperature, oxygen saturation level  
15 (%O<sub>2</sub>), concentrations of chlorophyll-*a* (Chl-*a*), total suspended matter (TSM), soluble reactive phosphorus (SRP), nitrite  
16 (NO<sub>2</sub><sup>-</sup>), nitrate (NO<sub>3</sub><sup>-</sup>), and ammonium (NH<sub>4</sub><sup>+</sup>). The turbid-water and clear-water ponds did not differ significantly in terms of  
17 diffusive emissions of CO<sub>2</sub> and N<sub>2</sub>O. Clear-water ponds exhibited higher values of ebullitive CH<sub>4</sub> emissions compared to  
18 turbid-water ponds, most probably in relation to the delivery of organic matter from macrophytes to sediments, but the  
19 diffusive CH<sub>4</sub> emissions were not significantly different between clear- and turbid-water ponds. These findings imply that it  
20 might be necessary to account for the presence of submerged macrophytes when scaling ebullitive CH<sub>4</sub> fluxes in ponds at  
21 larger scale (regional or global) (particularly if Chl-*a* is used as a descriptor), although possibly less critical for diffusive  
22 CH<sub>4</sub>, CO<sub>2</sub>, and N<sub>2</sub>O fluxes. At seasonal scale, CH<sub>4</sub> emissions increased with water temperature in all four ponds, with  
23 ebullitive CH<sub>4</sub> fluxes having a stronger dependence on water temperature (Q<sub>10</sub>) than diffusive CH<sub>4</sub> fluxes. The temperature  
24 sensitivity of ebullitive CH<sub>4</sub> fluxes decreased with increasing water depth, implying that shallow sediments would respond  
25 more strongly to warming (e.g. heat waves). Total annual CH<sub>4</sub> emissions (diffusive+ebullitive) in CO<sub>2</sub> equivalents equalled  
26 those of CO<sub>2</sub> in turbid-water ponds and exceeded those of CO<sub>2</sub> in clear-water ponds, while N<sub>2</sub>O emissions were negligible  
27 compared to the other two GHGs. Total annual GHG emissions in CO<sub>2</sub> equivalents from all four ponds increased from 2022  
28 to 2023 due to higher CO<sub>2</sub> diffusive fluxes, likely driven by higher annual precipitation in 2023 compared to 2022 (leading  
29 putatively to higher inputs for organic or inorganic carbon from run-off), possibly in response to the intense El Niño event of  
30 2023.

31 **1. Introduction**

32 Greenhouse gas (GHG) emissions from inland water (rivers, lakes, and reservoirs) to the atmosphere such as carbon dioxide  
33 (CO<sub>2</sub>), methane (CH<sub>4</sub>), and nitrous oxide (N<sub>2</sub>O) are quantitatively important for global budgets (Lauerwald et al., 2023).  
34 GHG emissions from lakes are lower than from rivers for CO<sub>2</sub> (Raymond et al., 2013) and for N<sub>2</sub>O (Lauerwald et al., 2019;  
35 Maavara et al., 2019). However, reported emissions of CH<sub>4</sub> from lakes (Rosentreter et al., 2021; Johnson et al., 2022) are  
36 equivalent or even higher compared to rivers (Stanley et al., 2016; Rocher-Ros et al., 2023). Emissions of CO<sub>2</sub> and CH<sub>4</sub> from

37 lakes to the atmosphere represent 1.25 to 2.30 Pg CO<sub>2</sub> equivalents (CO<sub>2</sub>-eq) annually with a significant proportion from CH<sub>4</sub>  
38 emissions, and represent nearly 20% of global CO<sub>2</sub> emissions from fossil fuels (Delsontro et al., 2018). The contribution of  
39 CO<sub>2</sub> and CH<sub>4</sub> emissions from small lentic water bodies (small lakes and ponds) can be disproportionately high compared to  
40 large systems (Holgerson and Raymond, 2016) as small lakes and ponds are the most abundant of all water body types in  
41 number (Verpoorter et al., 2014; Cael et al., 2017), and fluxes (per m<sup>2</sup>) are usually higher in smaller water bodies. The  
42 emissions of GHGs from artificial water bodies such as agricultural reservoirs, urban ponds, and storm-water retention  
43 basins could be higher than those from natural systems (Martinez-Cruz et al., 2017; Grinham et al., 2018; Herrero Ortega et  
44 al., 2019; Gorsky et al., 2019; Ollivier et al., 2019; Peacock et al., 2019, 2021; Webb et al., 2019; Bauduin et al., 2024).  
45 These higher emissions seem to result from higher external inputs of anthropogenic carbon and nitrogen into artificial  
46 systems, e.g. with rainfall runoff that brings organic matter and dissolved inorganic nitrogen (DIN), but might also reflect  
47 other differences compared to natural systems such as in hydrology (Clifford and Heffernan, 2018). Among artificial  
48 systems, urban ponds are the subject of a growing body of literature on GHG emissions (Singh et al., 2000; Natchimuthu et  
49 al., 2014; van Bergen et al., 2019; Audet et al., 2020; Peacock et al., 2021; Goeckner et al., 2022; Ray and Holgerson, 2023;  
50 Ray et al. 2023; Bauduin et al., 2024). Urban areas can have numerous small artificial water bodies mostly associated to  
51 green spaces such as public parks, and their number is increasing due to rapid urbanisation worldwide (Brans et al., 2018;  
52 Audet et al., 2020; Gorsky et al., 2024; Rabaey et al., 2024). Urban ponds are generally small, shallow, and usually their  
53 catchment consists in majority of impervious surfaces with a smaller contribution from soils (Davidson et al., 2015; Peacock  
54 et al., 2021). In general, the main function of urban ponds is for storm-water management but provide additional benefits  
55 including aesthetic/recreational amenities and habitats for wildlife (e.g. Tixier et al., 2011; Hassall, 2014).

56 Shallow ponds and lakes occur in two alternative states corresponding to systems with either clear waters (macrophyte-  
57 dominated) or turbid waters (phytoplankton-dominated), during the productive period of the year (spring and summer in  
58 mid-latitudes) (Scheffer et al., 1993). Submerged macrophytes and phytoplankton regulate CO<sub>2</sub> dynamics directly through  
59 photosynthesis that can be more or less balanced by community respiration in the water column (e.g., Sand-Jensen and  
60 Staehr, 2007). However, it is not clear whether the presence of macrophytes increases or decreases the net CO<sub>2</sub> emissions  
61 from ponds and lakes. Some studies have shown a decrease of CO<sub>2</sub> emissions with increasing macrophyte density (Kosten et  
62 al., 2010; Ojala et al., 2011; Davidson et al., 2015), but other studies showed the opposite pattern (Theus et al., 2023). In  
63 phytoplankton-dominated lakes, CO<sub>2</sub> concentrations depend in part on the developmental stage of phytoplankton, with the  
64 growth and peak phases generally coinciding with lower CO<sub>2</sub> concentrations due to photosynthesis (Grasset et al., 2020;  
65 Vachon et al., 2020).

66 CH<sub>4</sub> emissions have been reported to increase with the concentration of chlorophyll-*a* (Chl-*a*) in phytoplankton-dominated  
67 lakes (DelSontro et al., 2018; Borges et al., 2022). The presence of macrophytes strongly affects CH<sub>4</sub> cycling in freshwaters  
68 (Bastviken et al., 2023) and vegetated littoral zones of lakes exhibit higher CH<sub>4</sub> emissions than non-vegetated zones  
69 (Hyvönen et al., 1998; Huttunen et al., 2003; Juutinen et al., 2003; Desrosiers et al., 2022; Theus et al., 2023). Macrophytes  
70 influence organic matter decomposition processes in sediments depending on the quality and quantity of plant matter they  
71 release into their environment (Reitsema et al., 2018; Grasset et al., 2019; Harpenslager et al., 2022; Theus et al., 2023). Yet,  
72 few studies have consistently compared CH<sub>4</sub> emissions in clear-water and turbid-water ponds (Hilt et al., 2017). A study in  
73 Argentina reported higher dissolved CH<sub>4</sub> concentrations in clear-water ponds with submerged macrophytes compared to  
74 turbid-water phytoplankton-dominated ponds, but no differences in measured CH<sub>4</sub> emissions (Baliña et al., 2023).

75 The production of  $\text{N}_2\text{O}$  predominantly occurs through microbial nitrification and denitrification that depend on DIN,  $\text{O}_2$   
76 levels, and temperature (Codispoti and Christensen, 1985; Mengis et al., 1997; Velthuis and Veraart, 2022). Competition for  
77 DIN between primary producers and  $\text{N}_2\text{O}$ -producing microorganisms can impact  $\text{N}_2\text{O}$  production. Additionally, the transfer  
78 of labile phytoplankton organic matter to sediments fuels benthic denitrification and impacts  $\text{N}_2\text{O}$  fluxes. Eutrophication is  
79 assumed to drive high  $\text{N}_2\text{O}$  emissions from lakes and ponds (Audet et al., 2020; Webb et al., 2021; Wang et al., 2021; Xie et  
80 al., 2024) but some lakes with elevated Chl-*a* concentrations can act as sinks of  $\text{N}_2\text{O}$  due to removal of  $\text{N}_2\text{O}$  by  
81 denitrification (Webb et al., 2019; Borges et al., 2022; 2023). The presence of macrophytes also strongly influences nitrogen  
82 cycling in sediments of lakes and ponds (Barko et al., 1991; Choudhury et al., 2018; Deng et al., 2020; Dan et al., 2021) and  
83 should in theory also affect  $\text{N}_2\text{O}$  emissions, although seldom investigated, and available studies provide contradictory  
84 conclusions.  $\text{N}_2\text{O}$  emissions have been shown to follow diurnal cycles of  $\text{O}_2$  concentrations in areas dominated by  
85 submerged macrophytes in Lake Wuliangsuhai (China) (Ni et al., 2022) and the seasonal cycle of aboveground biomass of  
86 emerged macrophytes (*Phragmites*) in Baiyangdian Lake (China) (Yang et al., 2012). On the contrary, a study showed there  
87 was no significant difference of  $\text{N}_2\text{O}$  production in sediments of macrophyte-rich (n=10) and macrophyte-free (n=12) lakes  
88 in subtropical China (Liu et al., 2018). There has been a very limited number of studies systematically investigating how  
89 emissions differ between ponds dominated by phytoplankton and those dominated by macrophytes (Baliña et al., 2023), and  
90 none investigating simultaneously  $\text{CO}_2$ ,  $\text{CH}_4$ , and  $\text{N}_2\text{O}$  emissions including both diffusive and ebullitive components.

91 The emissions from aquatic systems of  $\text{CO}_2$  and  $\text{N}_2\text{O}$  are exclusively through diffusion across the air-water interface  
92 (diffusive flux), while  $\text{CH}_4$  can be additionally emitted as bubbles released from sediments to the atmosphere (ebullitive  
93 flux). At annual scale, ebullitive  $\text{CH}_4$  flux usually represents more than half of total (diffusive+ebullitive)  $\text{CH}_4$  emissions  
94 from shallow lakes (Wik et al., 2013; Deemer and Holgerson, 2021), although the relative contribution of ebullitive and  
95 diffusive  $\text{CH}_4$  emissions is highly variable seasonally (e.g. Wik et al., 2013; Ray and Holgerson, 2023; Rabaey and Cotner  
96 2024). Ebullitive  $\text{CH}_4$  fluxes are particularly high in the littoral zone of lakes at depths <5 m (Wik et al., 2013; DelSontro et  
97 al., 2016; Borges et al., 2022) and strongly increase in response to temperature (DelSontro et al., 2016; Aben et al., 2017;  
98 Rabaey and Cotner 2024), as well as organic matter availability (DelSontro et al., 2016; 2018). Ebullitive  $\text{CH}_4$  fluxes tend to  
99 be higher in small and shallow water bodies (Deemer and Holgerson, 2021) but are notoriously variable in time and space,  
100 and are difficult to estimate reliably (DelSontro et al., 2011).

101 Here, we report a dataset of  $\text{CO}_2$ ,  $\text{CH}_4$ , and  $\text{N}_2\text{O}$  dissolved concentrations in four shallow and small urban ponds (Leybeek,  
102 Pêcheries, Silex, and Tenreuken) in the city of Brussels (Belgium) (Fig. 1), with data collected 46 times at regular intervals  
103 (between June 2021 and December 2023) on each pond. The air-water diffusive fluxes of  $\text{CO}_2$ ,  $\text{CH}_4$ , and  $\text{N}_2\text{O}$  were  
104 calculated from dissolved concentrations and the gas transfer velocity, while the ebullitive  $\text{CH}_4$  fluxes were measured with  
105 inverted funnels during 8 deployments (totalling 48 days) in the four ponds. The four ponds have similar depth, surface area,  
106 and catchment urban coverage, and mainly differ by the phytoplankton-macrophyte dominance, a clear-water state  
107 dominated by macrophytes and a turbid-water state dominated by phytoplankton (alternative states) (Fig. 1). We test whether  
108 the differences between the four ponds are explained by the two alternative states in terms of (i)  $\text{CO}_2$ ,  $\text{CH}_4$ , and  $\text{N}_2\text{O}$   
109 dissolved concentration and diffusive emissions; (ii) ebullitive  $\text{CH}_4$  emissions; (iii) relative contribution of  $\text{CO}_2$ ,  $\text{CH}_4$ , and  
110  $\text{N}_2\text{O}$  to the total GHG emissions in  $\text{CO}_2\text{-eq}$ .

111 **2. Material and Methods**

112 **2.1. Field sampling and meteorological data**

113 Sampling was carried out from a pontoon in the four ponds on the same day between 9am and 11am, 46 times on each pond  
114 between June 2021 and December 2023 at a frequency ranging from one (winter) to three (summer) times per month at a  
115 single fixed station in each of the four ponds. Water was sampled 5 cm below the surface with 60 ml polypropylene syringes  
116 for analysis of dissolved concentrations of CO<sub>2</sub>, CH<sub>4</sub>, and N<sub>2</sub>O. Samples for CH<sub>4</sub> and N<sub>2</sub>O were transferred from the syringes  
117 with a silicone tube into 60 ml borosilicate serum bottles (Wheaton), preserved with 200 µl of a saturated solution of HgCl<sub>2</sub>,  
118 sealed with a butyl stopper and crimped with aluminium cap, without a headspace, and stored at ambient temperature in the  
119 dark prior to analysis in laboratory. The partial pressure of CO<sub>2</sub> (pCO<sub>2</sub>) was measured directly in the field, within 5 minutes  
120 of sample collection, with a Li-Cor Li-840 infrared gas analyser (IRGA) based on the headspace technique with 4  
121 polypropylene syringes (Borges et al., 2019). A volume of 30 ml of sample water was equilibrated with 30 ml of atmospheric  
122 air within the syringe by shaking vigorously for 5 minutes. The headspace of each syringe was then sequentially injected into  
123 the IRGA and a fifth syringe was used to measure atmospheric CO<sub>2</sub>. The final pCO<sub>2</sub> value was computed taking into account  
124 the partitioning of CO<sub>2</sub> between water and the headspace, as well as equilibrium with HCO<sub>3</sub><sup>-</sup> (Dickson et al., 2007) using  
125 water temperature measured in-situ and after equilibration, and total alkalinity (data not shown). Samples for total alkalinity  
126 were conditioned, stored, and analysed as described by Borges et al. (2019). The IRGA was calibrated in the laboratory with  
127 ultrapure N<sub>2</sub> and a suite of gas standards (Air Liquide Belgium) with CO<sub>2</sub> mixing ratios of 388, 813, 3788 and 8300 ppm.  
128 The precision of pCO<sub>2</sub> measurements was  $\pm 2.0\%$ . Water temperature, specific conductivity, and oxygen saturation level  
129 (%O<sub>2</sub>) were measured in-situ with VWR MU 6100H probe 5 cm below the surface. A 2 liter polyethylene water container  
130 was filled with surface water for conditioning the samples for other variables at the laboratory in Université Libre de  
131 Bruxelles.

132 Surveys to identify and quantify visually the relative coverage of emerged and submerged macrophytes were conducted in  
133 summer 2023 (Table S1). The resulting list of macrophyte species agreed with past studies in Brussels' ponds (Peretyatko et  
134 al., 2007).

135 Three bubble traps were deployed 50 cm apart for measuring ebullitive CH<sub>4</sub> flux. The bubble traps consisted of inverted  
136 polypropylene funnels (diameter 23.5 cm) mounted with 60 ml polypropylene syringes, with three way stop valves allowing  
137 to collect the gas without contamination from ambient air. The polypropylene funnel was attached with steel rods to a  
138 polystyrene float. The volume of gas collected in the funnels was sampled with graduated polypropylene 60 ml syringes  
139 every 24 hours. The value of the collected volume of gas was logged, and the gas was transferred immediately after  
140 collection to pre-evacuated 12 ml vials (Exetainers, Labco, UK) that were stored at ambient temperature in the dark prior to  
141 the analysis of CH<sub>4</sub> concentration in the laboratory. The time-series of measurements was longer at the Silex pond than the  
142 other three ponds, because the Silex pond is closed to the public during the week, while the other three ponds are open to the  
143 public all the time.

144 Air temperature, precipitation, wind speed, and atmospheric pressure, were retrieved from <https://wow.meteo.be/en> for the  
145 meteorological station of the Royal Meteorological Institute of St-Lambert (50.8408°N, 4.4234°E) in Brussels, located  
146 between 2.5 and 5.0 km from the surveyed ponds. Air temperature, wind speed and atmospheric pressure were averaged over  
147 24 h to obtain a daily mean value. Precipitation was integrated each day to obtain cumulated daily rainfall.

148 **2.2. Laboratory analysis**

149 **2.2.1. Chlorophyll-a, total suspended matter, and dissolved inorganic nutrients**

150 Water was filtered through Whatman GF/F glass microfiber filters (porosity 0.7  $\mu\text{m}$ ) with a diameter of 47 mm for total  
151 suspended matter (TSM) and Chl-a. Filters for TSM were dried in an oven at 50  $^{\circ}\text{C}$  and filters for Chl-a were kept frozen (-  
152 20  $^{\circ}\text{C}$ ). The weight of each filter was determined before and after filtration of a known volume of water using an Explorer<sup>TM</sup>  
153 Pro EP214C analytical microbalance (accuracy  $\pm 0.1$  mg) for determination of TSM concentration. Chl-a concentration was  
154 measured on extracts with 90% acetone by fluorimetry (Kontron model SFM 25) (Yentsch and Menzel, 1963) with a limit of  
155 detection of 0.01  $\mu\text{g L}^{-1}$ . Filtered water was stored frozen (-20  $^{\circ}\text{C}$ ) in 50 ml polypropylene bottles for analysis of dissolved  
156 nutrients. Soluble reactive phosphorus (SRP) was determined by the ammonium molybdate, ascorbic acid and potassium  
157 antimony tartrate staining method (Koroleff, 1983), with a limit of detection of 0.1  $\mu\text{mol L}^{-1}$ . Ammonium ( $\text{NH}_4^+$ ) was  
158 determined by the nitroprusside-hypochlorite-phenol staining method (Grasshoff and Johannsen, 1972), with a limit of  
159 detection of 0.05  $\mu\text{mol L}^{-1}$ . Nitrite ( $\text{NO}_2^-$ ) and nitrate ( $\text{NO}_3^-$ ) were determined before and after reduction of  $\text{NO}_3^-$  to  $\text{NO}_2^-$  by a  
160 cadmium-copper column, using the Griess acid reagent staining method (Grasshoff et al., 2009), with a detection limit of  
161 0.01 and 0.1  $\mu\text{mol L}^{-1}$ , respectively. Concentration of dissolved inorganic nitrogen (DIN) was calculated as the sum of  $\text{NH}_4^+$ ,  
162  $\text{NO}_2^-$  and  $\text{NO}_3^-$  concentrations in  $\mu\text{mol L}^{-1}$ .

163 **2.2.2.  $\text{CH}_4$  and  $\text{N}_2\text{O}$  measurements by gas chromatography**

164 Measurements of  $\text{N}_2\text{O}$  and  $\text{CH}_4$  concentrations dissolved in water and in the gas samples from bubbles were made with the  
165 headspace technique (Weiss, 1981) with an headspace volume of 20 ml of ultra-pure  $\text{N}_2$  (Air Liquid Belgium) and a gas  
166 chromatograph (GC) (SRI 8610C) with a flame ionisation detector for  $\text{CH}_4$  and an electron capture detector for  $\text{N}_2\text{O}$   
167 calibrated with  $\text{CH}_4:\text{N}_2\text{O}:\text{N}_2$  gas mixtures (Air Liquide Belgium) with mixing ratios of 1, 10 and 30 ppm for  $\text{CH}_4$ , and 0.2,  
168 2.0 and 6.0 ppm for  $\text{N}_2\text{O}$ . The precision of measurement based on duplicate samples was  $\pm 3.9\%$  for  $\text{CH}_4$  and  $\pm 3.2\%$  for  $\text{N}_2\text{O}$ .

169 The  $\text{CO}_2$  concentration is expressed as partial pressure ( $\text{pCO}_2$ ) in parts per million (ppm) and  $\text{CH}_4$  as dissolved concentration  
170 ( $\text{nmol L}^{-1}$ ), as frequently used in topical literature.  $\text{CH}_4$  concentration were systematically and distinctly above saturation  
171 level (2-3  $\text{nmol L}^{-1}$ ) and  $\text{pCO}_2$  values were below saturation only five times out of the 187 measurements. The  $\text{N}_2\text{O}$   
172 concentrations fluctuated around atmospheric equilibrium, so data are presented as percent of saturation level (% $\text{N}_2\text{O}$ , where  
173 atmospheric equilibrium corresponds to 100%). The equilibrium with atmosphere for  $\text{N}_2\text{O}$  was calculated from the average  
174 air mixing ratios of  $\text{N}_2\text{O}$  provided by the Global Monitoring Division (GMD) of the National Oceanic and Atmospheric  
175 Administration (NOAA) Earth System Research Laboratory (ESRL) (Dutton and Hall, 2023), and using the Henry's  
176 constant given by Weiss and Price (1980).

177 **2.3. Calculations**

178 **2.3.1. Diffusive GHG emissions**

179 The diffusive air-water  $\text{CO}_2$ ,  $\text{CH}_4$ , or  $\text{N}_2\text{O}$  fluxes ( $F_G$ ) were computed according to:

$$180 F_G = k \times \Delta[G], \quad (1)$$

181 where  $k$  is the gas transfer velocity and  $\Delta[G]$  is the air-water gas concentration gradient.

182 The atmospheric pCO<sub>2</sub> was measured in the field with the Li-Cor Li-840. For CH<sub>4</sub>, the global average present day  
 183 atmospheric mixing ratio of 1.9 ppm was used (Lan et al., 2024). Atmospheric N<sub>2</sub>O concentration was calculated from the  
 184 average air mixing ratios of N<sub>2</sub>O provided by the GMD of the NOAA ESRL (Dutton et al., 2017). *k* was computed from a  
 185 value normalized to a Schmidt number of 600 (*k*<sub>600</sub>) and from the Schmidt number of CO<sub>2</sub>, CH<sub>4</sub> and N<sub>2</sub>O in freshwater  
 186 according to the algorithms as function of water temperature given by Wanninkhof (1992). *k*<sub>600</sub> was calculated from the  
 187 parameterization as a function of wind speed of Cole and Caraco (1998). CH<sub>4</sub> and N<sub>2</sub>O emissions were converted into CO<sub>2</sub>  
 188 equivalents (CO<sub>2</sub>-eq) considering a 100-year timeframe, using global warming potentials of 32 and 298 for CH<sub>4</sub> and N<sub>2</sub>O,  
 189 respectively (Myrhe et al., 2013).

190 **2.3.2. Ebullitive flux**

191 Bubble flux (ml m<sup>-2</sup> d<sup>-1</sup>) measured with the inverted funnels was calculated according to:

$$192 F_{bubble} = \frac{V_g}{A \times \Delta t}, \quad (2)$$

193 where *V<sub>g</sub>* is the volume of gas collected in the funnels (ml), *A* is the cross-sectional area of the funnel (m<sup>2</sup>), *Δt* is the  
 194 collection time (d).

195 A multiple linear regression model of *F<sub>bubble</sub>* dependent on water temperature and drops of atmospheric pressure was fitted to  
 196 the data according to:

$$197 \log_{10}(F_{bubble}) = \alpha \times T_w + \beta \times \Delta p + \gamma, \quad (3)$$

198 where  $\alpha$  and  $\beta$  are the slope coefficients of the multiple linear regression model,  $\gamma$  is the y-intercept, *T<sub>w</sub>* is the water  
 199 temperature (°C), and  $\Delta p$  quantifies the drops in atmospheric pressure (atm), calculated according to Zhao et al. (2017):

$$200 \Delta p = -\frac{1}{\Delta t} \int_0^t p - p_0 ; \quad \forall p < p_0, \quad (4)$$

201 where *p* is the atmospheric pressure (atm), *p<sub>0</sub>* a threshold pressure fixed at 1 atm and *Δt* the time interval between two  
 202 measurements (d) (Fig. S1).

203 Ebullitive CH<sub>4</sub> fluxes (mmol m<sup>-2</sup> d<sup>-1</sup>) were calculated according to:

$$204 E_{CH4} = [CH_4] \times F_{bubble}, \quad (5)$$

205 where [CH<sub>4</sub>] is the CH<sub>4</sub> concentration in bubbles (mmol ml<sup>-1</sup>).

206 The methane ebullition Q<sub>10</sub> represents the proportional change in the ebullitive CH<sub>4</sub> flux per 10°C change in water  
 207 temperature (DelSontro et al., 2016) and was computed according to:

$$208 Q_{10} = 10^{10b}, \quad (6)$$

209 where *b* is the slope of the linear regression between the logarithm of the ebullitive CH<sub>4</sub> flux (*E<sub>CH4</sub>*) and *T<sub>w</sub>*, and *c* is the y-  
 210 intercept, according to:

$$211 \log_{10}(E_{CH4}) = b \times T_w + c, \quad (7)$$

212 **2.4. Statistical analysis**

213 For the data-sets covering the whole sampling period, for pCO<sub>2</sub>, dissolved CH<sub>4</sub> concentration, %N<sub>2</sub>O, bubble flux, %CH<sub>4</sub> in  
214 bubbles, and both ebullitive and diffusive CH<sub>4</sub> fluxes, generalized linear mixed models (GLMMs) were constructed that  
215 included water temperature, rainfall, %O<sub>2</sub>, Chl-*a*, TSM, DIN, SRP as fixed effects, and “pond” and “sampling date” as a  
216 random effect to account for repeated measurements via the *lme4* package (Bates et al., 2015) in R version 4.4.1 (R Core  
217 Team, 2021). When comparing data among the four ponds, “sampling date” was used as a random effect and post-hoc tests  
218 were performed using estimated marginal means (*emmeans* package) to assess pairwise differences between ponds.

219 For comparisons between the four seasons, GLMMs did not converge due to insufficient number of data points.  
220 Comparisons on log-transformed data were then made using repeated measures Analysis of variance (ANOVA) with  
221 Tukey’s honestly significant difference (HSD) post-hoc tests.

222 The relationships between the annual means of CH<sub>4</sub>, CO<sub>2</sub> and N<sub>2</sub>O fluxes and the annual means of a subset of variables (Chl-  
223 *a*, macrophyte cover, surface area, depth) were tested with Pearson’s linear or quadratic regressions. The modelled bubble  
224 fluxes in Silex pond were compared to measured values with Pearson’s linear regression.

225 Statistical significance was set at  $p < 0.05$  for all analyses. For comparisons presented on boxplots, different lower-case  
226 letters indicate a significant difference between groups.

227 **3. Results**

228 **3.1. Seasonal variations of meteorological conditions and GHG concentrations**

229 The city of Brussels experiences a temperate climate with mild weather year-round, and evenly distributed abundant rainfall  
230 totalling on average 837 mm annually for the reference period 1991-2020. The average annual air temperature was 11 °C,  
231 with summer average of 17.9 °C and winter average of 4.1 °C for the reference period 1991-2020. During the sampling  
232 period, from June 2021 to December 2023, water temperature in the surface of the four sampled ponds (Leybeek, Pêcheries,  
233 Silex, and Tenreuken; Fig. 1) tracked closely the air temperature that ranged between -1.5 and 30.0°C following the typical  
234 seasonal cycle at mid-latitudes in the Northern Hemisphere (Fig. S2). Years 2022 and 2023 were about 1 °C warmer than the  
235 average for the period 1991-2020 (11 °C), while year 2021 was closer to the long-term average (Fig. 2). Year 2022 was  
236 warmer and drier than 2021 and 2023 (Fig. 2), with positive air temperature anomalies observed evenly throughout the year  
237 (9 months out of 12) and negative precipitation anomalies in summer, fall, and early winter (Fig. S2). Year 2021 had warmer  
238 and drier months in June and September, colder and wetter months in July and August, and was overall wetter and colder  
239 than 2022 (Fig. 2). Year 2023 was marked by both positive air temperature and precipitation anomalies (Fig. S2), resulting in  
240 a wetter and warmer year than normal and compared to 2021 and 2022 (Fig. 2). Daily wind speed was generally low ( $<1 \text{ m s}^{-1}$ )  
241 except for a windier period in spring 2022 (up to 5.8 m s<sup>-1</sup>, corresponding to the Eunice storm) and in fall 2023 (up to 9.7  
242 m s<sup>-1</sup>, corresponding to the Ciarán storm) (Fig. S2).

243 The four sampled ponds are situated in the periphery of the city of Brussels, with the Silex pond bordered by the Sonian  
244 Forest (Fig. 1). The four ponds are relatively small (0.7-3.2 ha) and shallow (0.6-1.4 m) and have not been drained or  
245 dredged since at least 2018 (Table S2). The four studied ponds had significantly different Chl-*a* concentration values during  
246 summer, with the Leybeek pond having higher Chl-*a* ( $78.8 \pm 49.5 \text{ } \mu\text{g L}^{-1}$ ), followed by the Pêcheries pond ( $19.1 \pm 13.7 \text{ } \mu\text{g L}^{-1}$ ),  
247 the Tenreuken pond ( $3.3 \pm 2.4 \text{ } \mu\text{g L}^{-1}$ ), and the Silex pond ( $1.0 \pm 1.2 \text{ } \mu\text{g L}^{-1}$ ) (Figs. 1, 3, Table S3). The Leybeek and Pêcheries

248 ponds with higher summer Chl-*a* concentration had turbid-water (summer TSM = 48.7±36.2 and 13.7±10.7 mg L<sup>-1</sup>,  
249 respectively), and undetectable submerged macrophyte cover in summer (Fig. 1, Table S1). The Tenreuken and Silex ponds  
250 with lower summer Chl-*a* concentrations had clear-water (summer TSM = 4.9±3.2 and 4.0±3.2 mg L<sup>-1</sup>, respectively), and a  
251 high total macrophyte cover during summer (68 and 100%, respectively, Fig. 1, Table S1). Seasonally, the highest values of  
252 Chl-*a* were observed in summer in the turbid-water Leybeek and Pêcheries ponds, related to algal blooms. Conversely,  
253 lowest values of Chl-*a* were observed in summer in the clear-water Tenreuken and Silex ponds (Figs. 1, 3), probably related  
254 to competition for inorganic nutrients from macrophytes.

255 The %O<sub>2</sub> values ranged from 11 to 191% (Fig. 3). The highest %O<sub>2</sub> values in the four ponds were observed in spring and  
256 summer compared to fall and winter owing to aquatic primary production. In summer, %O<sub>2</sub> was significantly higher in the  
257 Leybeek pond (109±46%) characterized by higher Chl-*a* concentration compared to the Pêcheries pond (75±23%, p=0.0212,  
258 Table S3). The lowest average %O<sub>2</sub> was observed in fall in the Pêcheries pond (46±22%) and was significantly lower than in  
259 the Leybeek (85±34%, p=0.0146, Table S3) and Silex ponds (81±19%, p=0.0130, Table S3).

260 The pCO<sub>2</sub> values ranged from 40 to 13,804 ppm (Fig. 3). Undersaturation of CO<sub>2</sub> with respect to atmospheric equilibrium  
261 was only observed on five occasions out of the 187 measurements, three times in the turbid-water Leybeek pond in summer  
262 (40 ppm on 13 August 2021, 220 ppm on 27 June 2022 and 149 ppm on 13 June 2023), and twice in the clear-water  
263 Tenreuken pond in spring and summer (383 ppm on 13 August 2021 and 55 ppm on 2 May 2022). Low values of pCO<sub>2</sub> were  
264 generally observed in spring and summer and high values of pCO<sub>2</sub> were observed in fall in the four ponds (Fig. 3). In  
265 summer, pCO<sub>2</sub> was lower in the Leybeek pond (2187±2012 ppm) than in the Pêcheries (3427±1672 ppm, p=0.0015, Table  
266 S3), and Silex (3222±1175 ppm, p=0.0002, Table S3) ponds. When data were pooled together, pCO<sub>2</sub> was correlated  
267 negatively with %O<sub>2</sub>, and positively with both DIN and SRP, and with precipitation (Table S4). In individual ponds, pCO<sub>2</sub>  
268 correlated negatively with %O<sub>2</sub> and positively with precipitation in the four ponds, positively with DIN in the Leybeek pond,  
269 with DIN and SRP in the Tenreuken pond, and negatively with Chl-*a* in the Silex pond (Table S5).

270 The CH<sub>4</sub> dissolved concentrations ranged from 194 to 48,380 nmol L<sup>-1</sup> (Fig. 3) and was always above saturation. High  
271 values of CH<sub>4</sub> dissolved concentrations were generally observed in spring and summer and low values of CH<sub>4</sub> dissolved  
272 concentrations were generally observed in winter in the four ponds (Fig. 3). In summer, CH<sub>4</sub> dissolved concentration was  
273 higher in the Silex pond (4898±3384 nmol L<sup>-1</sup>) than in the Pêcheries (2518±2105 nmol L<sup>-1</sup>, p=0.0385, Table S3) and  
274 Tenreuken (2189±1365 nmol L<sup>-1</sup>, p=0.0055, Table S3) ponds. When data were pooled together, dissolved CH<sub>4</sub> concentration  
275 was positively correlated with water temperature (Table S4). In individual ponds, CH<sub>4</sub> dissolved concentration was  
276 positively correlated with water temperature in the four ponds (Table S5). Additionally, CH<sub>4</sub> dissolved concentration was  
277 correlated positively with precipitation in the Leybeek pond, negatively with DIN in the Pêcheries pond, negatively with  
278 Chl-*a* in the Tenreuken pond, and negatively with Chl-*a* and positively with SRP in the Silex pond (Table S5). These  
279 relationships between CH<sub>4</sub> and other variables probably indirectly reflect the seasonal variations of these other variables that  
280 also correlated with water temperature. DIN was correlated negatively with water temperature in the Pêcheries pond, Chl-*a*  
281 was negatively correlated with temperature in the Tenreuken pond, and SRP was positively and Chl-*a* negatively correlated  
282 with water temperature in the Silex pond (Table S6).

283 The %N<sub>2</sub>O values ranged from 32 to 826% (Fig. 3). Undersaturation of N<sub>2</sub>O with respect to atmospheric equilibrium was  
284 observed 66 times out of the 187 measurements. Low values of %N<sub>2</sub>O were generally observed in spring and summer and  
285 high values of %N<sub>2</sub>O were generally observed in fall and winter in the four ponds (Fig. 3). During spring, the %N<sub>2</sub>O was  
286 lower in the Pêcheries pond (90±11%) than the Leybeek (138±30%, p=0.0043, Table S3) and the Tenreuken (138±41,

287 p=0.0057, Table S3) ponds. During summer, the %N<sub>2</sub>O was lower in the Pêcheries pond (78±17%) than the Leybeek  
288 (191±104%, p<0.0001, Table S3) and the Silex (126±49%, p=0.001, Table S3) pond, and lower in the Tenreuken pond  
289 (133±106%) than the Leybeek pond (p=0.0219, Table S3). During fall, %N<sub>2</sub>O was lower in the Pêcheries pond (103±33%)  
290 than the Leybeek pond (190±70%, p=0.0174, Table S3). For the all sampling period, %N<sub>2</sub>O was lower in the Pêcheries pond  
291 (94±28%) than the Leybeek (178±82 %, p<0.0001, Table S7), Tenreuken (140±77%, p<0.0001, Table S7) and Silex  
292 (144±113%, p<0.0001, Table S7) ponds, and was lower in the Tenreuken pond than the Leybeek pond (p=0.0038, Table S7).  
293 When data were pooled together, %N<sub>2</sub>O was correlated negatively with water temperature and positively with DIN and NH<sub>4</sub><sup>+</sup>  
294 (Table S4). In individual ponds, %N<sub>2</sub>O was negatively correlated with water temperature in the Leybeek, Pêcheries, and  
295 Tenreuken ponds (Table S5). %N<sub>2</sub>O was positively correlated with NO<sub>3</sub><sup>-</sup> in the Leybeek pond and with NH<sub>4</sub><sup>+</sup> in the Pêcheries  
296 and Tenreuken ponds (Table S8). %N<sub>2</sub>O was positively correlated with Chl-*a* and TSM in the Tenreuken pond, and  
297 negatively with Chl-*a* in the Leybeek pond (Table S5), probably reflecting the negative correlation of Chl-*a* and TSM with  
298 water temperature in the Tenreuken pond and the positive correlation of Chl-*a* with water temperature in the Leybeek pond  
299 (Table S6).

### 300 3.2. Drivers of bubble flux

301 The bubble flux measured with inverted funnels in the four sampled ponds in the city of Brussels ranged between 0 and 2078  
302 ml m<sup>-2</sup> d<sup>-1</sup> and was positively correlated with water temperature (Fig. 4). The mean CH<sub>4</sub> content of the bubbles in the four  
303 sampled ponds in the city of Brussels was 31±21%, and values were positively correlated with water temperature (Fig. 4).  
304 The CH<sub>4</sub> content of the bubbles was correlated with bubble flux (Fig. S3) as both variables correlated positively with water  
305 temperature (Fig. 4).

306 The bubble fluxes were measured during more lengthy series at the Silex pond than the other three ponds for logistical  
307 reasons allowing investigating the effects of water temperature and atmospheric pressure variations on bubble fluxes in more  
308 detail. In spring 2022, the bubble flux at the Silex pond increased during events of drops in atmospheric pressure  
309 (depressions) (Fig. 5). There was no relation between wind speed and peaks of bubble flux ( $r^2 = 0.01$ , p=0.4629), suggesting  
310 a more important role of changes of atmospheric pressure than wind speed in the Silex pond in spring 2022. The bubble flux  
311 at the Silex pond was higher in summer (1152±433 mL m<sup>-2</sup> d<sup>-1</sup>) than during spring (198±170 mL m<sup>-2</sup> d<sup>-1</sup>) and the temporal  
312 changes of bubble fluxes tracked those of water temperature (Fig. 5). The bubble flux was modelled as function of water  
313 temperature alone or as function of both water temperature and atmospheric pressure changes (Figs. 5, S4). For periods of  
314 low temperature (<15°C), the inclusion of the term of air pressure drops in the model improved the performance of the  
315 model by comparison to the measurements (Figs. 5, S4). But for warmer periods (>15°C), when bubbling fluxes were  
316 quantitatively more important, the inclusion of the term of air pressure drops in the model did not improve the performance  
317 of the model (Figs. 5, S4). For the full temperature range (<15°C and >15°C), the inclusion of the term of air pressure drops  
318 only improved the performance of the model very marginally (Fig. S4).

### 319 3.3. Drivers of methane ebullitive fluxes

320 Ebullitive CH<sub>4</sub> fluxes in the four ponds ranged between 0 and 59 mmol m<sup>-2</sup> d<sup>-1</sup> and were positively related to water  
321 temperature (Fig. 6). The fitted relations between ebullitive CH<sub>4</sub> fluxes and water temperature were specific to each pond  
322 and encompassed the fitted relations established in similar systems: four small ponds in Québec (DelSontro et al., 2016) and  
323 a small urban pond in the Netherlands (Aben et al., 2017). The Q<sub>10</sub> of CH<sub>4</sub> ebullition values ranged between 4.4 in the deeper  
324 Pêcheries pond and 26.9 in the shallower Leybeek pond, respectively (Table S9). The Q<sub>10</sub> of CH<sub>4</sub> ebullition in the four

325 studied ponds of the city of Brussels, in Québec (DelSontro et al., 2016), and in the Netherlands (Aben et al., 2017) were  
326 negatively related to water depth (Fig. 6).

327 **3.4. Relative contribution of methane ebullitive and diffusive fluxes**

328 Diffusive CH<sub>4</sub> fluxes computed from dissolved CH<sub>4</sub> concentration and *k* derived from wind speed ranged between 0.1 and  
329 19.7 mmol m<sup>-2</sup> d<sup>-1</sup> (Fig. 7). The diffusive CH<sub>4</sub> fluxes tended to be higher in summer and spring than in fall and winter owing  
330 to the strong positive dependency between CH<sub>4</sub> dissolved concentration and water temperature (Fig. 3; Tables S4, S5). In  
331 addition, wind speed only showed small seasonal variations during sampling (0.6±0.6 m s<sup>-1</sup> in spring, 0.3±0.2 m s<sup>-1</sup> in  
332 summer, 0.7±0.7 m s<sup>-1</sup> in fall, and 0.6±0.2 m s<sup>-1</sup> in winter) (Fig. S2). Ebullitive CH<sub>4</sub> fluxes were calculated from the relations  
333 with water temperature for each pond given in Figure 6 from the water temperature data coincident with the diffusive CH<sub>4</sub>  
334 fluxes (Fig. 7). The resulting calculated ebullitive CH<sub>4</sub> fluxes allowed to compare and integrate seasonally both components  
335 of CH<sub>4</sub> emissions to the atmosphere, and to calculate the relative contribution of ebullition to total (diffusive+ebullitive) CH<sub>4</sub>  
336 emissions. The relative contribution of ebullition to total CH<sub>4</sub> emissions ranged between 1 and 99% in the four sampled  
337 ponds in the city of Brussels (Fig. 7) and was positively correlated to water temperature (Fig. S5). The values of Q<sub>10</sub> of  
338 diffusive CH<sub>4</sub> fluxes were lower than those for ebullitive CH<sub>4</sub> fluxes in each pond, and less variable (1.2 in the Pêcheries  
339 pond to 2.9 in the Silex pond) (Table S9).

340 The annually averaged diffusive and ebullitive fluxes of CH<sub>4</sub> in the four ponds in the city of Brussels were plotted against  
341 annually averaged Chl-*a* concentration, total macrophyte cover in summer, water depth, and lake surface area (Fig. 8) that  
342 are frequent predictors of variations of CH<sub>4</sub> fluxes among lakes (Holgerson and Raymond, 2016; DelSontro et al., 2018,  
343 Deemer and Holgerson, 2021; Casas-Ruiz et al., 2021; Borges et al., 2022). The annually averaged ebullitive CH<sub>4</sub> fluxes  
344 were significantly higher in the two clear-water ponds (7.3±2.9 and 13.4±3.7 mmol m<sup>-2</sup> d<sup>-1</sup> in the Tenreuken and Silex ponds,  
345 respectively) than the two turbid-water ponds (3.8±3.2 and 2.5±1.4 mmol m<sup>-2</sup> d<sup>-1</sup> in the Leybeek and Pêcheries ponds,  
346 respectively) (Table S7). The annually averaged ebullitive CH<sub>4</sub> fluxes were significantly higher in the Silex pond, that  
347 showed a higher macrophyte cover during summer (100% in the Silex pond and 68% in the Tenreuken pond), than the  
348 Tenreuken pond (p<0.0001, Table S7) and were not significantly different in the two turbid-water Leybeek and Pêcheries  
349 ponds (p=0.0617, Table S7) that showed similar macrophyte cover during summer (6 and 9% in the Leybeek and Pêcheries  
350 ponds, respectively) (Fig. 8). The annually averaged ebullitive CH<sub>4</sub> fluxes were overall positively correlated with  
351 macrophyte cover and negatively correlated with Chl-*a* (Fig. 8).

352 In the four sampled urban ponds, annually averaged CH<sub>4</sub> diffusive fluxes were higher in the pond with the highest total  
353 macrophyte cover in the clear-water ponds, and higher in the pond with the highest Chl-*a* concentration in the turbid-water  
354 ponds (Fig. 8). The annually averaged relative contribution of ebullition to total CH<sub>4</sub> emissions were higher in the two clear-  
355 water ponds than the two turbid-water ponds (Table S7). The relative contribution of ebullitive CH<sub>4</sub> fluxes to the total CH<sub>4</sub>  
356 flux seems to increase concomitantly with the macrophyte cover (Fig. 8), and was overall positively correlated with  
357 macrophyte cover and negatively to Chl-*a* (Fig. 8).

358 The annually averaged diffusive fluxes of CO<sub>2</sub> (F<sub>CO2</sub>) and N<sub>2</sub>O (F<sub>N2O</sub>) in the four ponds in the city of Brussels were also  
359 plotted against annually averaged Chl-*a* concentration, total macrophyte cover in summer, water depth, and lake surface area  
360 (Fig. S6). Annually averaged F<sub>CO2</sub> were lower in the Leybeek pond than the Pêcheries and Silex ponds (Table S7). F<sub>CO2</sub> did  
361 not significantly correlate with the other variables (Chl-*a* concentration, total macrophyte cover, water depth, and lake  
362 surface area) (Fig. S6). Annually averaged F<sub>N2O</sub> was not significantly different between clear-water and turbid-water ponds.

363  $F_{N2O}$  was significantly lower in the slightly deeper Pêcheries pond than the two slightly shallower Leybeek and Silex ponds  
364 (Table S7), and  $F_{N2O}$  showed a significant negative relationship with water depth (Fig. S6).

365 **3.5. Relative contribution of CO<sub>2</sub>, CH<sub>4</sub> and N<sub>2</sub>O emissions**

366 The emissions in CO<sub>2</sub>-eq for the 3 GHGs averaged per season for both 2022 and 2023 peaked seasonally in summer with 2.9  
367 and 1.7 mg CO<sub>2</sub>-eq m<sup>-2</sup> d<sup>-1</sup> in the Silex and the Tenreuken ponds, respectively, and 1.1 mg CO<sub>2</sub>-eq m<sup>-2</sup> d<sup>-1</sup> in the Leybeek  
368 pond (Fig. 9). The GHG fluxes in CO<sub>2</sub>-eq peaked in fall in the Pêcheries pond, with 1.3 mg CO<sub>2</sub>-eq m<sup>-2</sup> d<sup>-1</sup>. The higher value  
369 of the total GHG emissions in fall compared to other seasons in the Pêcheries pond was due to an increase of CO<sub>2</sub> emissions  
370 in fall that surpassed the peak of CH<sub>4</sub> emissions in summer. The GHG fluxes were the lowest in winter with 1.3 and 0.9 mg  
371 CO<sub>2</sub>-eq m<sup>-2</sup> d<sup>-1</sup> in the Silex and the Tenreuken ponds, respectively, and 0.8 and 0.6 mg CO<sub>2</sub>-eq m<sup>-2</sup> d<sup>-1</sup> in the Pêcheries and the  
372 Leybeek ponds, respectively. The relative contribution of ebullitive CH<sub>4</sub> fluxes peaked in summer in all four ponds,  
373 73.8% and 70.9% in the Silex and the Tenreuken ponds, respectively, and 23.6% and 58.3% in the Pêcheries and the  
374 Leybeek ponds, respectively. The relative contribution of ebullitive CH<sub>4</sub> fluxes was the lowest in winter with 22.1% and  
375 10.0% in the Silex and the Tenreuken ponds, respectively, and 6.7% and 1.0% in the Pêcheries and the Leybeek ponds,  
376 respectively.

377 The annual emissions in CO<sub>2</sub>-eq of the three GHGs (CO<sub>2</sub>, CH<sub>4</sub>, and N<sub>2</sub>O) in 2022 and 2023 were higher in the two clear-  
378 water ponds (1.3±0.5 and 1.8±0.9 mg CO<sub>2</sub>-eq m<sup>-2</sup> d<sup>-1</sup> in the Tenreuken and Silex ponds, respectively) than in the two turbid-  
379 water ponds (1.0±0.2 and 0.9±0.5 mg CO<sub>2</sub>-eq m<sup>-2</sup> d<sup>-1</sup> in the Leybeek and Pêcheries ponds, respectively) (Fig. 9) due to higher  
380 total CH<sub>4</sub> emissions (diffusive+ebullitive) in clear-water ponds (0.7±0.4 and 1.2±0.5 mg CO<sub>2</sub>-eq m<sup>-2</sup> d<sup>-1</sup> in the Tenreuken and  
381 Silex ponds, respectively) than in turbid-water ponds (0.2±0.2 and 0.4±0.3 mg CO<sub>2</sub>-eq m<sup>-2</sup> d<sup>-1</sup> in the Leybeek and Pêcheries  
382 ponds, respectively). The contribution of N<sub>2</sub>O to the total GHG emissions was marginal and did not affect the differences in  
383 total GHG fluxes between ponds, with the highest contribution observed in the Leybeek pond, with a contribution of 1.7%.

384 The majority of GHG emissions in CO<sub>2</sub>-eq was related to CO<sub>2</sub> and CH<sub>4</sub> (diffusive+ebullitive) in the four ponds. In turbid-  
385 water ponds CO<sub>2</sub> represented the largest fraction of GHG emissions (68.5% (2022) and 79.3% (2023) in the Pêcheries pond,  
386 and 49.0% (2022) and 58.3% (2023) in the Leybeek pond). In clear-water ponds CH<sub>4</sub> represented the largest fraction of  
387 GHG emissions (66.5% (2022) and 63.3% (2023) in the Silex pond, and 60.8% (2022) and 50.0% (2023) in the Tenreuken  
388 pond). The higher annual GHG emissions in CO<sub>2</sub>-eq from the two clear-water ponds than the turbid-water ponds were  
389 related to the higher contribution of ebullitive CH<sub>4</sub> fluxes.

390 The annual GHG fluxes increased from 2022 to 2023 due to an increase in relative contribution of CO<sub>2</sub> diffusive emissions  
391 in all four ponds. Diffusive CO<sub>2</sub> emissions averaged annually in all four ponds 0.5 mg CO<sub>2</sub> m<sup>-2</sup> d<sup>-1</sup> in 2022 and 0.7 mg CO<sub>2</sub>  
392 m<sup>-2</sup> d<sup>-1</sup> in 2023. Diffusive CO<sub>2</sub> emissions were 2.1 times higher in summer 2023 than in summer 2022, and 2.5 times higher  
393 in fall 2023 than in fall 2022, and showed similar values between 2023 and 2022 in spring and winter (1.1 higher and 1.1  
394 lower, respectively).

395 **4. Discussion**

396 The Leybeek and Pêcheries ponds are turbid-water systems (high Chl-*a* and TSM values, low submerged macrophyte cover)  
397 and the Tenreuken and Silex ponds are clear-water systems (low Chl-*a* and TSM values, high submerged macrophyte cover)  
398 (Figs. 1, 3). All four ponds have a relatively similar size (0.7 to 3.2 ha) and depth (0.5 to 1.4 m) and are uniformly located in  
399 an urban landscape in the city of Brussels. It can be assumed that, among the four systems, the major difference that is

400 expected to affect GHG emissions is the dominance of aquatic primary producer, either phytoplankton or macrophytes,  
401 corresponding to two alternative states *sensu* Scheffer et al. (1993). Our data-set provides the opportunity to test the effect of  
402 the two alternative states on GHG emissions from small lentic systems.

403 The reported pCO<sub>2</sub> values (40 to 13,804 ppm) (Fig. 3) in the four ponds in the city of Brussels were within the range of  
404 values typically observed in ponds (Holgerson and Raymond, 2016; Peacock et al., 2019; Audet et al., 2020) (Fig. 3). The  
405 pCO<sub>2</sub> values were correlated negatively with %O<sub>2</sub> and positively with DIN and SRP across seasons (Tables S4, S5) showing  
406 that their seasonal variability was driven by aquatic primary production and degradation of organic matter (*e.g.* Holgerson  
407 2015). Low values of pCO<sub>2</sub> were generally observed in spring and summer probably due to uptake of CO<sub>2</sub> by primary  
408 production from either phytoplankton or submerged macrophytes. High values of pCO<sub>2</sub> were observed in fall in the four  
409 ponds and probably reflect the release of CO<sub>2</sub> from degradation of organic matter due to the senescence of phytoplankton or  
410 macrophytes (Fig. 3). In all four ponds, pCO<sub>2</sub> values were positively correlated with precipitation (Tables S4, S5) suggesting  
411 an additional control of external inputs of carbon either as organic carbon sustaining internal degradation of organic matter  
412 or as soil CO<sub>2</sub> (*e.g.* Marotta et al., 2010; Ojala et al., 2011; Rasilo et al., 2012; Vachon and del Giorgio, 2014; Holgerson,  
413 2015). The %N<sub>2</sub>O values (32 to 826%) (Fig. 3) in the four ponds were within the range typically observed in ponds (Audet et  
414 al., 2020; Rabaey and Cotner, 2022). When pooled all the data together, %N<sub>2</sub>O was positively correlated with DIN (Table  
415 S4) as frequently reported by other studies in ponds and interpreted as a control of nitrification and/or denitrification (hence  
416 N<sub>2</sub>O production) by DIN levels (Audet et al., 2020; Webb et al., 2021; Wang et al., 2021; Xie et al., 2024). The negative  
417 correlation between %N<sub>2</sub>O with temperature (Table S4) might reflect the effect of the inhibition at low temperatures of the  
418 final step of denitrification leading to an accumulation of N<sub>2</sub>O (Velthuis and Veraart, 2022) but could also indirectly result  
419 from the higher DIN values at low temperatures (Table S6). The CH<sub>4</sub> dissolved concentrations (194 to 48,380 nmol L<sup>-1</sup>) (Fig.  
420 3) in the four ponds were within the range of values typically observed in ponds (Natchimuthu et al., 2014; Holgerson and  
421 Raymond, 2016; Peacock et al., 2019; Audet et al., 2020; Rabaey and Cotner, 2022; Ray et al., 2023), and were positively  
422 correlated with water temperature in all four ponds and when pooled all the data together (Tables S4, S5), most probably  
423 reflecting the increase of sedimentary methanogenesis with temperature (Schulz and Conrad, 1996).

424 Temperature also exerted a strong control on bubble flux from sediments and ebullitive CH<sub>4</sub> emissions. The bubble flux  
425 values (0 and 2078 ml m<sup>-2</sup> d<sup>-1</sup>) in the four sampled ponds (Fig. 4) were within the range of values reported in lentic systems  
426 of equivalent size by Wik et al. (2013) (0 to 2772 mL m<sup>-2</sup> d<sup>-1</sup>), Delsontro et al. (2016) (11 to 748 mL m<sup>-2</sup> d<sup>-1</sup>), and Ray and  
427 Holgerson (2023) (0 to 2079 mL m<sup>-2</sup> d<sup>-1</sup>). The bubble flux was positively correlated with water temperature (Fig. 4) in  
428 agreement with previous studies (*e.g.* Wik et al., 2013; DelSontro et al., 2016; Aben et al., 2017; Ray and Holgerson, 2023).  
429 Bubbling events from lake sediments are known to also be triggered by a decrease of hydrostatic pressure on the sediments  
430 due to water level fluctuations or drops in atmospheric pressure (Tokida et al., 2007; Scandella et al., 2011; Varadharajan  
431 and Hemond, 2012; Wik et al., 2013; Taoka et al., 2020; Zhao et al., 2021). In the Silex pond, in spring 2022, some peaks in  
432 bubble fluxes were related to drops in atmospheric pressure (Fig. 5) but unrelated to wind speed ( $r^2 = 0.01$ ,  $p=0.4629$ ) as  
433 shown in Gatun Lake (Keller and Stallard, 1994). A statistical model of the bubble flux that included the contributions of  
434 water temperature and air pressure drops was used to quantify the relative importance of each of these two drivers (Fig. S4).  
435 The contribution of the air pressure drop seemed quantitatively important only at low water temperature (<15°C) and was  
436 negligible at higher water temperature (>15°C) (Fig. S4). The inclusion of the term of air pressure drops only improved the  
437 performance of the model compared to the original data very marginally when comparing across the full water temperature  
438 range (<15°C and >15°C) (Fig. S4), showing that the intensity of bubble flux was mainly driven by temperature change at

439 yearly scales, in agreement with previous studies (e.g. Wik et al., 2013; DelSontro et al., 2016; Aben et al., 2017; Ray and  
440 Holgerson, 2023).

441 The mean CH<sub>4</sub> content of the bubbles (31±21%) in the four sampled ponds in the city of Brussels was comparable to the  
442 values obtained by Wik et al. (2013) (35±25%), DelSontro et al. (2016) (58±25%), and Ray and Holgerson (2023) (25±13%)  
443 in lentic systems of equivalent size. The increasing pattern of the CH<sub>4</sub> content of the bubbles with water temperature (Fig. 4)  
444 was most probably related to the strong dependence of methanogenesis on temperature (Schulz and Conrad, 1996). The  
445 increase of methanogenesis with temperature leads to the build-up of gas bubbles in sediments that are richer in CH<sub>4</sub>, and  
446 consequently to higher bubble fluxes with a higher CH<sub>4</sub> content at higher temperatures (Figs. 4, S3). Since both bubble flux  
447 and the CH<sub>4</sub> content of the bubbles increased with water temperature (Fig. 4), the ebullitive CH<sub>4</sub> fluxes in the four ponds  
448 were also positively related to water temperature (Fig. 6) as shown previously in other small lentic systems (e.g. Wik et al.,  
449 2013; DelSontro et al., 2016; Natchimuthu et al., 2016; Aben et al., 2017; Ray and Holgerson, 2023; Rabaey and Cotner,  
450 2024). Yet, the dependency of CH<sub>4</sub> ebullition on temperature ( $Q_{10}$ ) was different among the four ponds and was negatively  
451 related to depth including data from systems in Québec (DelSontro et al., 2016) and the Netherlands (Aben et al., 2017) (Fig.  
452 6). This implies that an increase in water temperature leads to a smaller increase in CH<sub>4</sub> ebullitive fluxes (lower  $Q_{10}$ ) in  
453 deeper ponds as the impact of hydrostatic pressure on sediments is higher in deeper ponds compared to shallow ponds,  
454 restricting bubble formation and release (e.g. DelSontro et al., 2016). This dependence of  $Q_{10}$  of CH<sub>4</sub> ebullition to depth  
455 suggests that the response of CH<sub>4</sub> ebullition to heatwaves (or longer-term warming) might be more intense the shallower the  
456 pond, in addition to other effects from heat-waves on GHG emissions (e.g. Audet et al., 2017).

457 The values of  $Q_{10}$  for diffusive CH<sub>4</sub> fluxes in the four ponds were lower than those for ebullitive CH<sub>4</sub> fluxes (Table S9) as  
458 reported by other studies in lentic systems (DelSontro et al., 2016; Xun et al., 2024). The lower dependence to water  
459 temperature of diffusive CH<sub>4</sub> fluxes compared to ebullitive CH<sub>4</sub> fluxes might be related to a lower relative change of CH<sub>4</sub>  
460 concentrations and  $k$  with the variation of water temperature. CH<sub>4</sub> concentrations in surface waters of lentic systems are  
461 strongly affected by microbial methane oxidation (e.g. Bastviken et al., 2002). A relative increase of CH<sub>4</sub> production in  
462 sediments by methanogenesis might lead to a stronger increase of CH<sub>4</sub> emission by ebullition than by diffusion because of a  
463 mitigation by methane oxidation on CH<sub>4</sub> diffusive fluxes. Additionally,  $k$  depends on wind speed, but in the four ponds, the  
464 warmer periods of the year (summer) tended to be less windy ( $\sim 0.3 \text{ m s}^{-1}$ ) than the other seasons ( $> 0.6 \text{ m s}^{-1}$ ) also  
465 contributing to a lower dependence on water temperature of CH<sub>4</sub> diffusive fluxes compared to ebullitive fluxes and lower  
466  $Q_{10}$  values.

467 The difference in the  $Q_{10}$  of diffusive and ebullitive CH<sub>4</sub> fluxes was consistent with a variable contribution of the diffusive  
468 and ebullitive CH<sub>4</sub> fluxes seasonally as a function of water temperature, with the contribution of ebullitive CH<sub>4</sub> fluxes  
469 strongly increasing with water temperature in the four ponds (Fig. S5). At annual scale, ebullitive CH<sub>4</sub> fluxes represented  
470 between 55% and 83% of the total CH<sub>4</sub> emissions in the Leybeek and Silex ponds, respectively. This finding is consistent  
471 with other studies showing that ebullitive CH<sub>4</sub> fluxes can account for more than half of total CH<sub>4</sub> emissions in small and  
472 shallow lentic systems (e.g. Wik et al., 2013; Deemer and Holgerson, 2021; Ray and Holgerson, 2023; Rabaey and Cotner,  
473 2024). The averaged ebullitive CH<sub>4</sub> emissions were higher in the two clear-water ponds ( $10.4 \text{ mmol m}^{-2} \text{ d}^{-1}$ ) than the two  
474 turbid-water ponds ( $3.2 \text{ mmol m}^{-2} \text{ d}^{-1}$ ) (Fig 7). The averaged ebullitive CH<sub>4</sub> emissions in the four ponds were positively  
475 correlated with macrophyte cover and negatively correlated with Chl-*a* (Fig. 8). The higher ebullitive CH<sub>4</sub> emissions from  
476 the two clear-water ponds would suggest that the delivery of organic matter to sediments from macrophytes sustained a  
477 quantitatively larger methane production than from phytoplankton. This finding is consistent with the notion that vegetated

478 littoral zones of lakes are hot spots of CH<sub>4</sub> production and emission (e.g. Hyvönen et al., 1998; Huttunen et al., 2003;  
479 Juutinen et al., 2003; Desrosiers et al., 2022). CH<sub>4</sub> fluxes in lentic systems have been scaled at globally scale assuming a  
480 dependency on aquatic productivity using Chl-*a* as a predictor (e.g. DelSontro et al., 2018). The negative relation between  
481 CH<sub>4</sub> ebullitive fluxes with Chl-*a* shows that Chl-*a* concentration alone fails to predict ebullitive fluxes in macrophyte-  
482 dominated clear-water ponds.

483 The annually averaged diffusive CH<sub>4</sub> emissions in the four ponds seemed to respond positively to both increasing  
484 phytoplankton and macrophyte biomass resulting in a U-shaped relation between diffusive CH<sub>4</sub> emissions and Chl-*a* as well  
485 as macrophyte cover (Fig. 8). Higher values of annually averaged CH<sub>4</sub> diffusive fluxes occurred at the extreme values of  
486 Chl-*a* or of macrophyte cover (minimum or maximum), and lower values occurred at the intermediate values of Chl-*a* or  
487 macrophyte cover. Such U-shape relation resulted from the anti-correlation between macrophyte cover and Chl-*a* (alternative  
488 states) and is consistent with reported positive relation between diffusive CH<sub>4</sub> fluxes with both macrophyte cover (e.g. Ray et  
489 al., 2023; Theus et al., 2023) as well as with phytoplankton biomass (e.g. DelSontro et al., 2018; Yan et al., 2019;  
490 Bartosiewicz et al., 2021). The relative contribution of ebullitive CH<sub>4</sub> fluxes to the total annual CH<sub>4</sub> flux increased with the  
491 macrophyte cover (Fig. 8), in agreement with the idea of an increase of CH<sub>4</sub> ebullition relative to diffusive CH<sub>4</sub> emissions in  
492 vegetated sediments compared to unvegetated sediments (e.g. Desrosiers et al., 2022; Ray et al., 2023; Theus et al., 2023).

493 Fluxes of CH<sub>4</sub> and CO<sub>2</sub> have been reported to be negatively related to surface area and depth by numerous studies in ponds  
494 (e.g. Holgerson, 2015; Holgerson and Raymond, 2016; Ray et al., 2023; Theus et al., 2023) and lakes (e.g. Kankaala et al.,  
495 2013; DelSontro et al., 2018, Deemer and Holgerson, 2021; Casas-Ruiz et al., 2021; Borges et al., 2022). Annual diffusive  
496 F<sub>CH<sub>4</sub></sub> and F<sub>CO<sub>2</sub></sub> were both unrelated to surface area and depth in the four studied ponds (Figs. 8, S6) resulting from the narrow  
497 range of variation of water depth (0.6 to 1.4 m) and surface area (0.7 to 3.2 ha). The lack of correlation between annual F<sub>CO<sub>2</sub></sub>  
498 and both Chl-*a* and macrophyte cover in the four ponds (Fig. S6) might be surprising since other studies have reported lower  
499 CO<sub>2</sub> fluxes in more productive lentic systems (e.g. Sand-Jensen and Staehr, 2007; Borges et al., 2022). We hypothesize that  
500 given that the four systems were either phytoplankton-dominated or macrophyte-dominated (alternative states), the ponds  
501 had an important submerged productivity, in both cases, resulting in a relatively invariant F<sub>CO<sub>2</sub></sub> as function of either Chl-*a* or  
502 macrophyte cover. Annual F<sub>N<sub>2</sub>O</sub> was negatively correlated with water depth (Fig. S6) which we hypothesize might reflect a  
503 larger dilution of N<sub>2</sub>O diffusing from sediments in the deeper systems.

504 Global average emissions of GHGs in CO<sub>2</sub>-eq from inland waters are dominated by CO<sub>2</sub> followed by CH<sub>4</sub> with a small  
505 contribution from N<sub>2</sub>O according to Lauerwald et al. (2023). However, in small lentic systems such as ponds, the  
506 contribution of CH<sub>4</sub> to CO<sub>2</sub>-eq emissions can match (e.g. Webb et al., 2023) or dominate (e.g. Ray and Holgerson, 2023;  
507 Rabaey and Cotner, 2024) the one of CO<sub>2</sub>. The meta-analysis of Holgerson and Raymond (2016) suggested that the CO<sub>2</sub> and  
508 CH<sub>4</sub> emissions in CO<sub>2</sub>-eq are numerically close in small lentic systems such as ponds but become increasingly dominated by  
509 CO<sub>2</sub> emissions with the augmentation of lake size. In the four studied ponds, the GHG emissions in CO<sub>2</sub>-eq were dominated  
510 by CO<sub>2</sub> and CH<sub>4</sub> with a marginal contribution (<1%) from N<sub>2</sub>O (Fig. 9). Annually, CO<sub>2</sub> represented the largest fraction of  
511 GHG emissions in CO<sub>2</sub>-eq (~60%) in turbid-water ponds (Leybeek and Pêcheries), while CH<sub>4</sub> represented the largest  
512 fraction of GHG emissions in CO<sub>2</sub>-eq (~60%) in clear-water ponds (Silex and Tenreuken) as a result of higher ebullitive CH<sub>4</sub>  
513 fluxes in the clear-water ponds (Fig. 7).

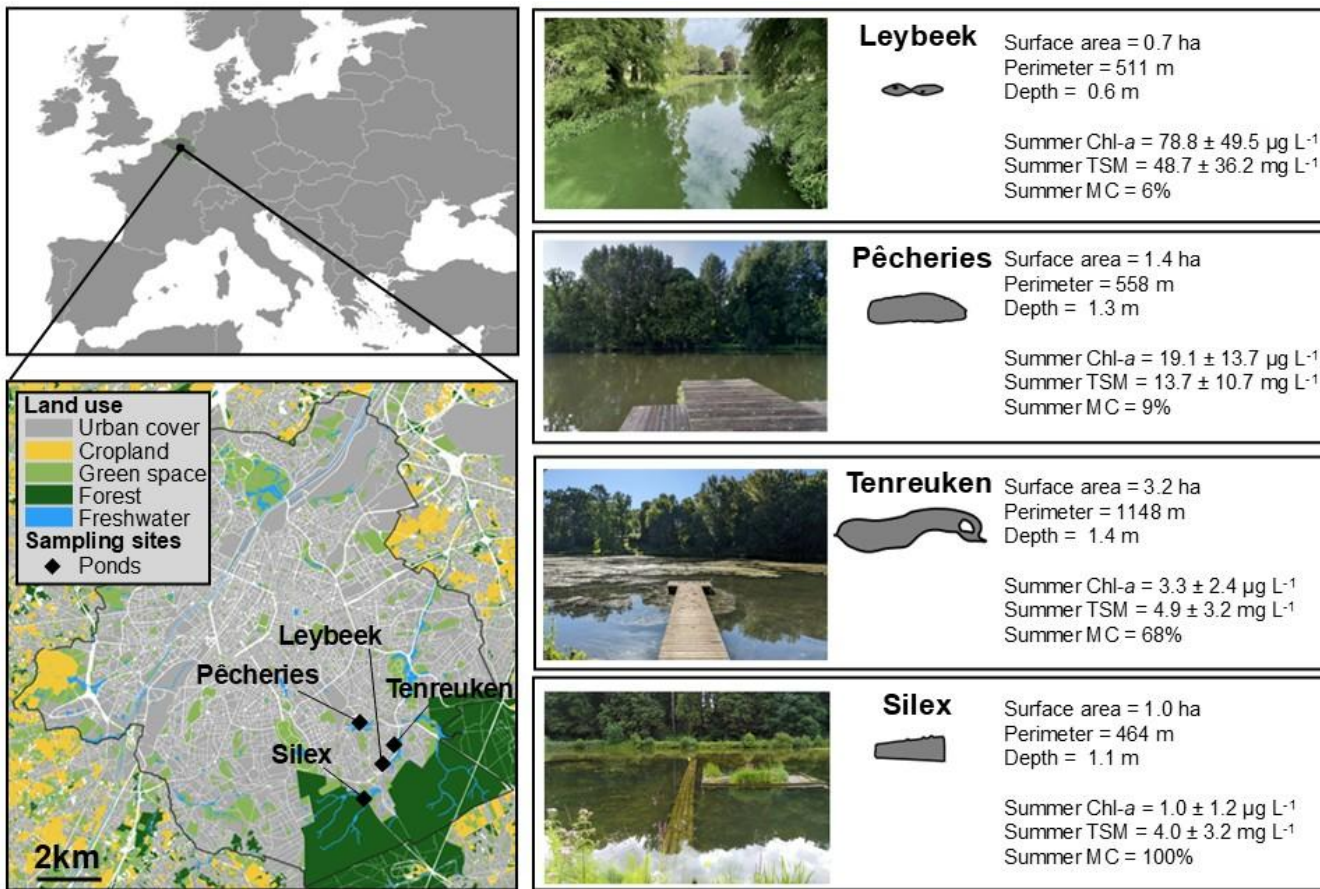
514 The annual GHG emissions in CO<sub>2</sub>-eq increased from 2022 to 2023 due to an increase in the relative contribution of CO<sub>2</sub>  
515 diffusive emissions in all four ponds (Fig. 9) as a result of higher precipitations in 2023 (Fig. 2). Air temperatures were  
516 similar in both years (annual average of 12.2°C in 2022 and 12.1°C in 2023), and precipitations were 1.5 times higher in

517 2023 than in 2022. Higher precipitations are likely to increase the inputs of organic and inorganic carbon from soils to ponds  
518 by ground-waters, soil-waters, and surface runoff, as previously shown in other lentic systems (*e.g.* Marotta et al., 2011;  
519 Ojala et al., 2011; Rasilo et al., 2012; Vachon and del Giorgio, 2014; Holgerson, 2015). While this hypothesis is only based  
520 on the comparison of two years, the increase of the relative contribution of CO<sub>2</sub> diffusive emissions in 2023 was observed in  
521 all four ponds which suggests a common uniform driver that would be consistent with a large variation weather such as  
522 annual precipitation. The El Niño event in 2023 induced low-level cyclonic wind anomalies and higher precipitation over  
523 Western Europe, including Belgium (Chen et al., 2024).

524 **5. Conclusions**

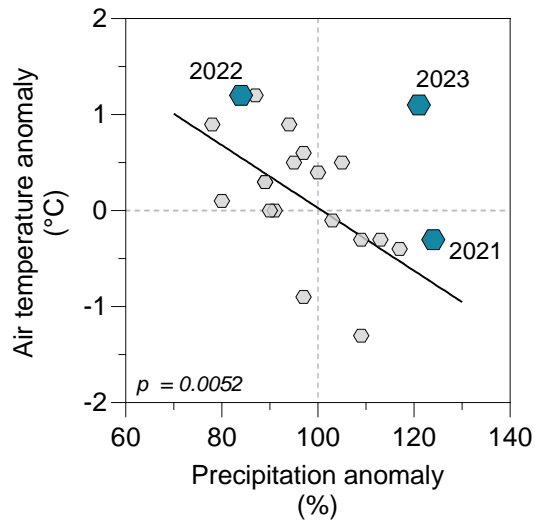
525 Ebullitive CH<sub>4</sub> emissions in 2022-2023 were higher in the two clear-water macrophyte-dominated ponds (Tenreuken and  
526 Silex) than in the two turbid-water phytoplankton-dominated ponds (Pêcheries and Leybeek) of the city of Brussels,  
527 although, the diffusive CH<sub>4</sub> fluxes were not systematically significantly different between the clear-water ponds and the  
528 turbid-water ponds. The annually averaged diffusive N<sub>2</sub>O and CO<sub>2</sub> fluxes were not significantly different in the two clear-  
529 water ponds from those in the two turbid-water ponds. Other studies have found no difference in N<sub>2</sub>O sedimentary  
530 production in lakes with high and low density of submerged macrophytes. We hypothesize that CO<sub>2</sub> fluxes were relatively  
531 invariant among the four sampled ponds because of they were of similar size and depth, and that they were all equivalently  
532 productive irrespective of whether from phytoplankton or submerged macrophytes. The total (diffusive and ebullitive) CH<sub>4</sub>  
533 emissions represented 58% of total annual GHG emissions in CO<sub>2</sub>-eq in the two clear-water ponds compared to 41% in the  
534 two turbid-water ponds. CO<sub>2</sub> represented nearly all the remainder of total annual GHG emissions in CO<sub>2</sub>-eq, and N<sub>2</sub>O  
535 represented a very marginal fraction (<1%).

536 The seasonal variations of GHG emissions were dominated by CH<sub>4</sub> ebullitive seasonal variations that peaked in summer  
537 (both quantitatively and relatively), as CH<sub>4</sub> ebullition was strongly related to water temperature resulting from an increase  
538 with water temperature in both flux of bubble and CH<sub>4</sub> content of bubble. The pCO<sub>2</sub> values in the four sampled ponds  
539 increased with precipitation at seasonal scale, probably in relation to higher inputs of organic and inorganic carbon by  
540 surface runoff. Years 2022 and 2023 were abnormally dry and wet, respectively, and consequently, the GHG emissions were  
541 higher in 2023 mainly due to an increase in the relative contribution of CO<sub>2</sub> emissions, probably in response to a strong El  
542 Niño event. This would suggest that variations of precipitation also affected year-to-year variations of CO<sub>2</sub> emissions in  
543 addition to partly regulating seasonal variations of CO<sub>2</sub> emissions from the four studied ponds.



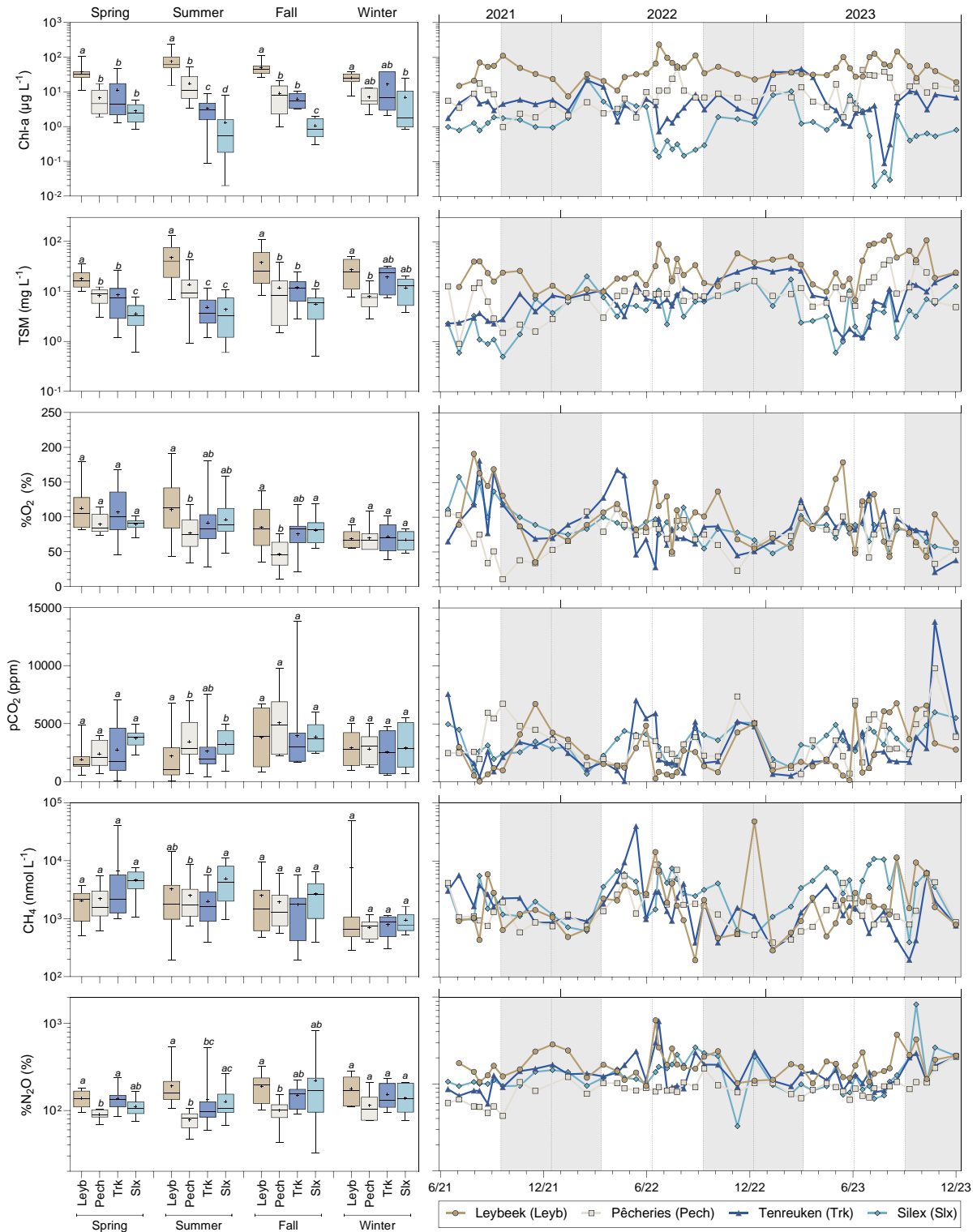
544

545 Figure 1: Location of the four sampled urban ponds (black diamonds) in city of Brussels (Belgium) delineated by the black line.  
 546 Right panels indicate for each pond the shape of the ponds, surface area (ha), perimeter (m), average depth (m), mean±standard  
 547 deviation of chlorophyll-a (Chl-a, in  $\mu\text{g L}^{-1}$ ) and total suspended matter (TSM, in  $\text{mg L}^{-1}$ ) in summer (21 June to 21 September in  
 548 2021, 2022, 2023), and summer total macrophyte cover (MC, in %) (Table S1).

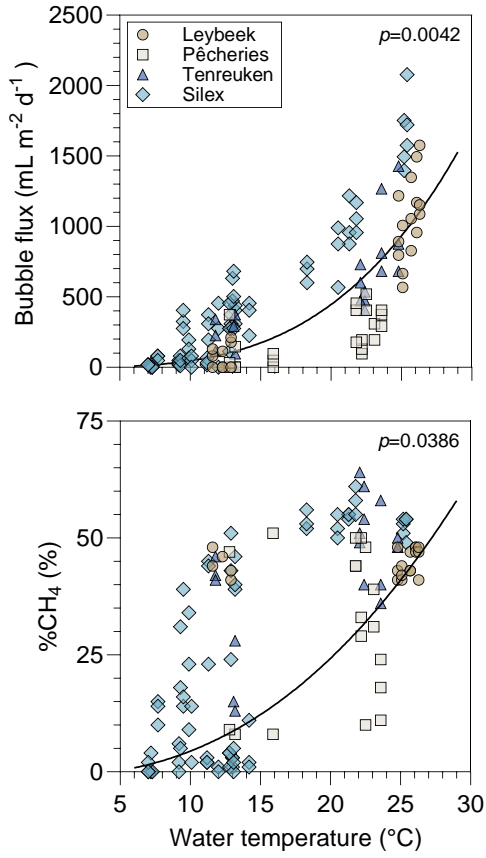


549

550 **Figure 2:** Anomaly of annual air temperature (°C) as a function of anomaly of annual precipitation (%) from 2003 to 2023 with  
 551 respect to average of the 1991-2020 period (11 °C and 837 mm, respectively). Each small grey hexagon represents values for years  
 552 from 2003 to 2020 and larger blue hexagons represent the years of sampling from this study (2021, 2022 and 2023). Linear  
 553 regression for years 2003-2020 is shown by a black solid line ( $Y = 3.29 - 0.03 \cdot X$ , n=20). Note the anomalous rainy year in 2023  
 554 relative to the pattern as function of temperature for the other years, possibly in response to the strong El Niño event of 2023  
 555 (Chen et al., 2024).

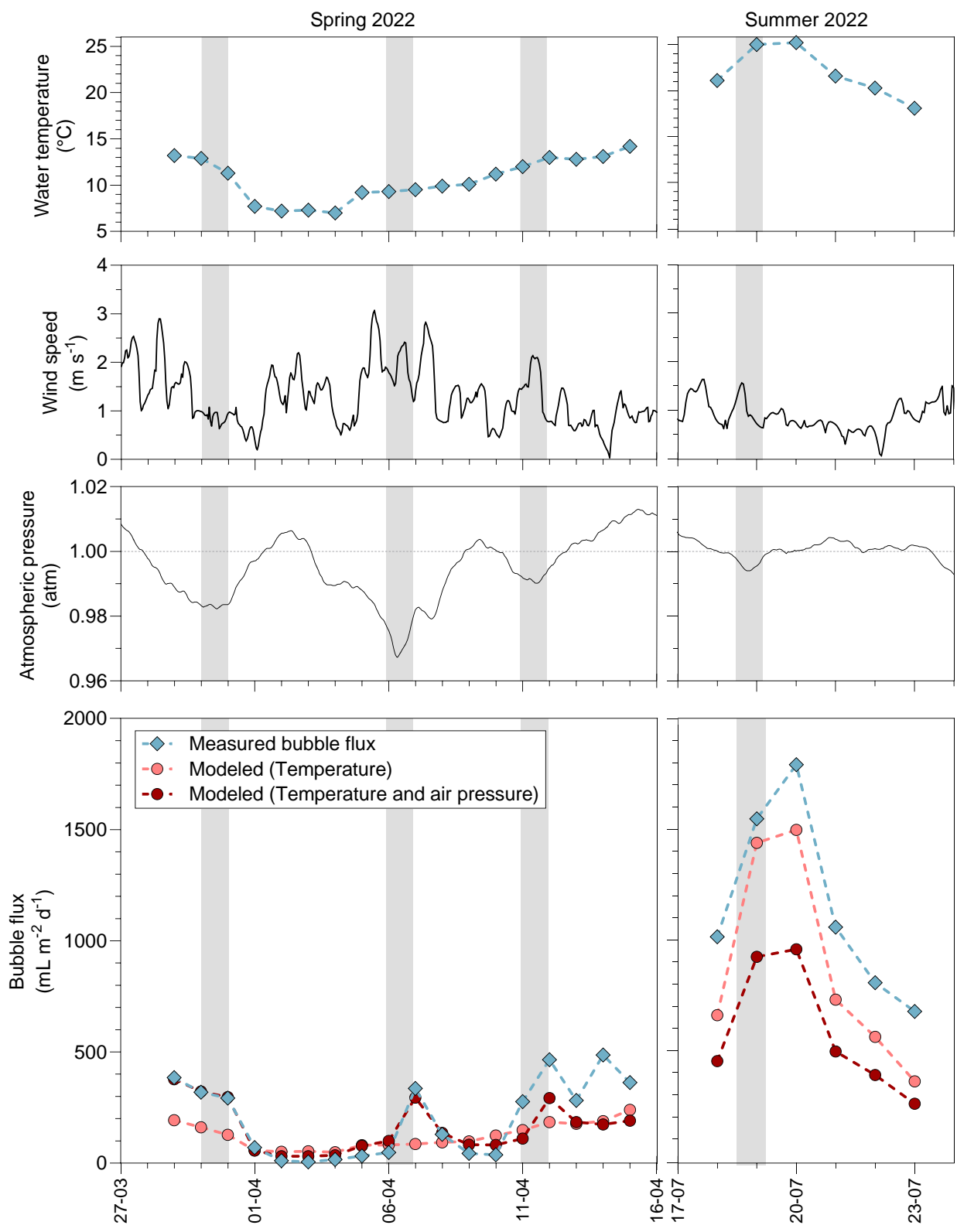


557 **Figure 3: Seasonal variations of Chlorophyll- $\alpha$  (Chl- $\alpha$ , in  $\mu\text{g L}^{-1}$ ), total suspended matter (TSM, in  $\text{mg L}^{-1}$ ), oxygen saturation (558  $\% \text{O}_2$ , in %), partial pressure of  $\text{CO}_2$  ( $\text{pCO}_2$  in ppm), dissolved  $\text{CH}_4$  concentration (559  $\text{CH}_4$ , in  $\text{nmol L}^{-1}$ ), and  $\text{N}_2\text{O}$  saturation level (560  $\% \text{N}_2\text{O}$ , in %) in four urban ponds (Leybeek (Leyb), Pêcheries (Pech), Tenreuken (Trk), and Silex (Slx)) in the city of Brussels 561 (Belgium) from June 2021 to December 2023. Box plots show median (horizontal line), mean (cross), and 25–75% 562 percentiles (box limits). Whiskers extend from minimum to maximum values. White and grey bands in the graphs on the right 563 correspond to the autumn/winter and spring/summer periods, respectively, and dotted vertical bars represent the first day of each 564 season. Lower case letters indicate significant differences between ponds (Tables S3 and S4).**

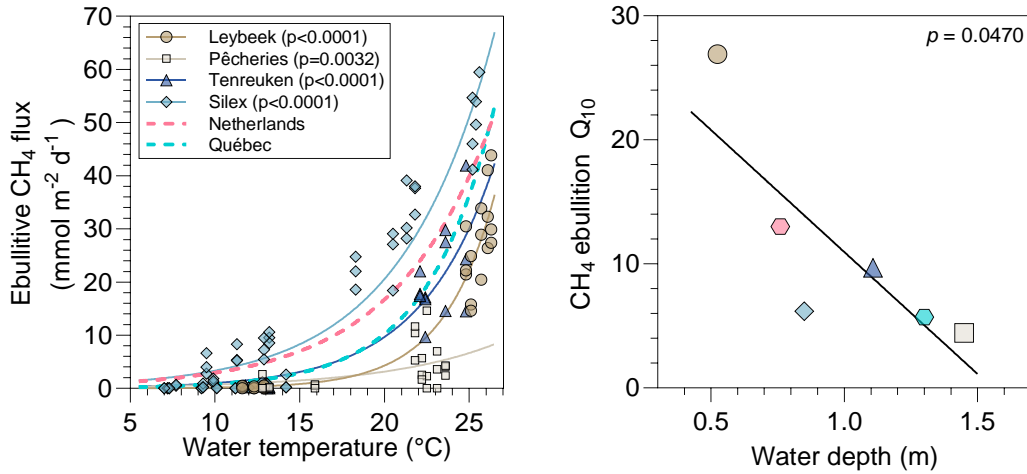


564

565 Figure 4: Bubble flux ( $\text{ml m}^{-2} \text{ d}^{-1}$ ) and the relative  $\text{CH}_4$  content in bubbles (% $\text{CH}_4$ , in %) as a function of surface water  
 566 temperature ( $^{\circ}\text{C}$ ) in four urban ponds (Leybeek, Pêcheries, Tenreuken, and Silex) in the city of Brussels (Belgium) from June 2021  
 567 to December 2023. Bubbles fluxes were measured with three bubble traps in spring, summer, and fall of 2022 and 2023, totalling 8  
 568 days in the Leybeek, Pêcheries, and Tenreuken ponds and 24 days in the Silex pond. Given the shallowness of the sampled systems  
 569 (<1.5 m, Fig. 1), we assume that sediments experience the same temperature as surface waters. Solid lines represent the predictions  
 570 of the GLMM considering the ponds and sampling dates as random effects for bubble flux as function of water temperature ( $Y = 0.0121 \times (1 + X)^{3.4538} - 1$ ), and % $\text{CH}_4$  as function of water temperature ( $Y = 0.0181 \times (1 + X)^{3.3783} - 1$ ).  
 571

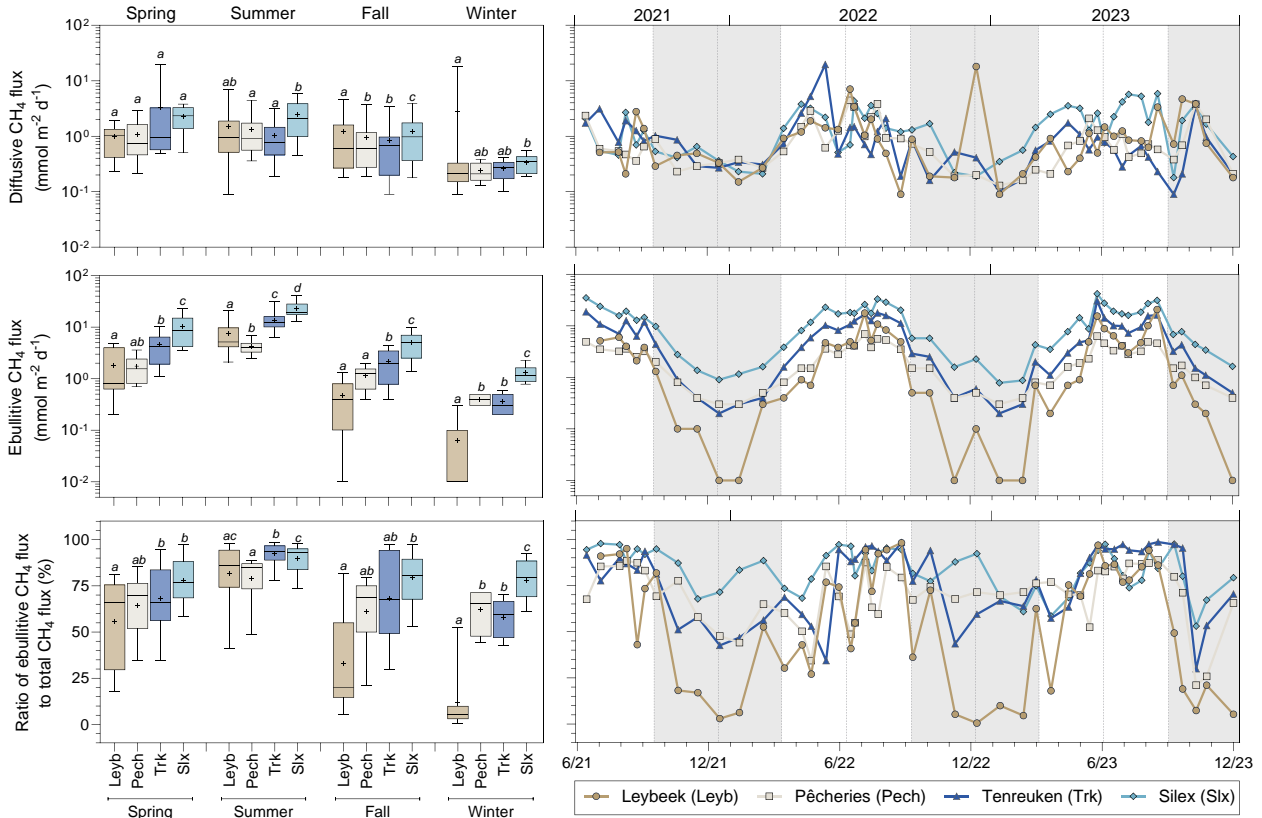


574 **Figure 5:** Surface water temperature (°C), wind speed (m s<sup>-1</sup>), atmospheric pressure (atm), measured and modeled bubble flux (ml  
 575 m<sup>-2</sup> d<sup>-1</sup>) in the Silex pond from the 29 March 2022 to the 15 April 2022 and from the 18 July 2022 to the 23 July 2022. The bubble  
 576 flux was modelled from a fit to data based on water temperature alone and based on both water temperature and drops in  
 577 atmospheric pressure.



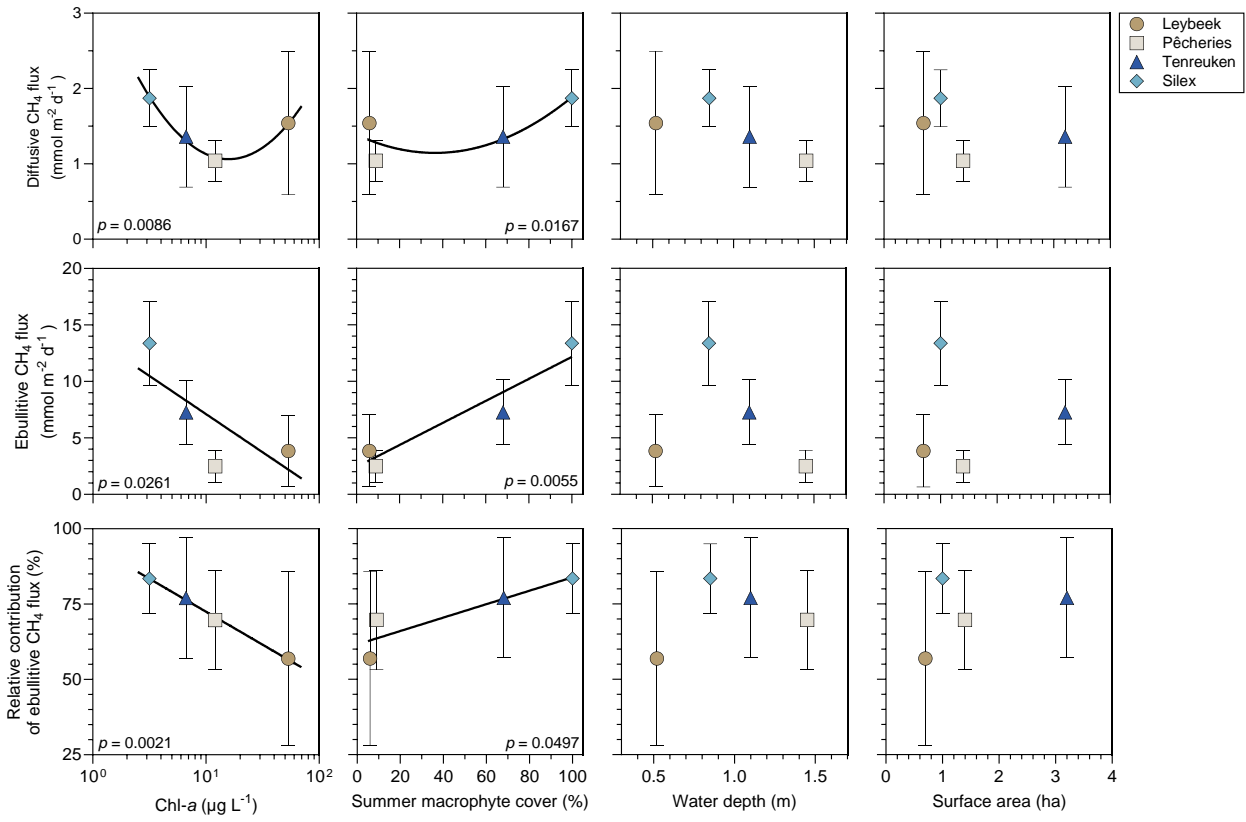
578

579 **Figure 6: Measured ebullitive CH<sub>4</sub> fluxes (mmol m<sup>-2</sup> d<sup>-1</sup>) as function of surface water temperature (°C) in four urban ponds**  
580 (Leybeek, Pêcheries, Tenreuken, and Silex) in the city of Brussels (Belgium), in spring, summer, and fall of 2022 and 2023,  
581 totalling 8 days in the Leybeek, Pêcheries, and Tenreuken ponds and 24 days in the Silex pond, with three bubble traps. Solid lines  
582 represent exponential fit for the Leybeek ( $Y = 0.01 \cdot e^{0.32 \cdot X}$ , n=22), Pêcheries ( $Y = 0.16 \cdot e^{0.15 \cdot X}$ , n=22), Tenreuken ( $Y =$   
583  $0.10 \cdot e^{0.23 \cdot X}$ , n=19), Silex ( $Y = 0.54 \cdot e^{0.18 \cdot X}$ , n=72) ponds (Table S7). Dashed lines represent published exponential fit  
584 established in similar systems: four small ponds in Québec ( $Y = 0.06 \cdot e^{0.25 \cdot X}$ ) (DelSontro et al., 2016) and a small urban pond in  
585 the Netherlands ( $Y = 0.51 \cdot e^{0.17 \cdot X}$ ) (Aben et al., 2017). Each exponential curve allows to determine a Q<sub>10</sub> of CH<sub>4</sub> ebullition,  
586 plotted against water depth; solid line represents linear regression ( $Y = 30.64 - 19.67 \cdot X$ , n = 6).



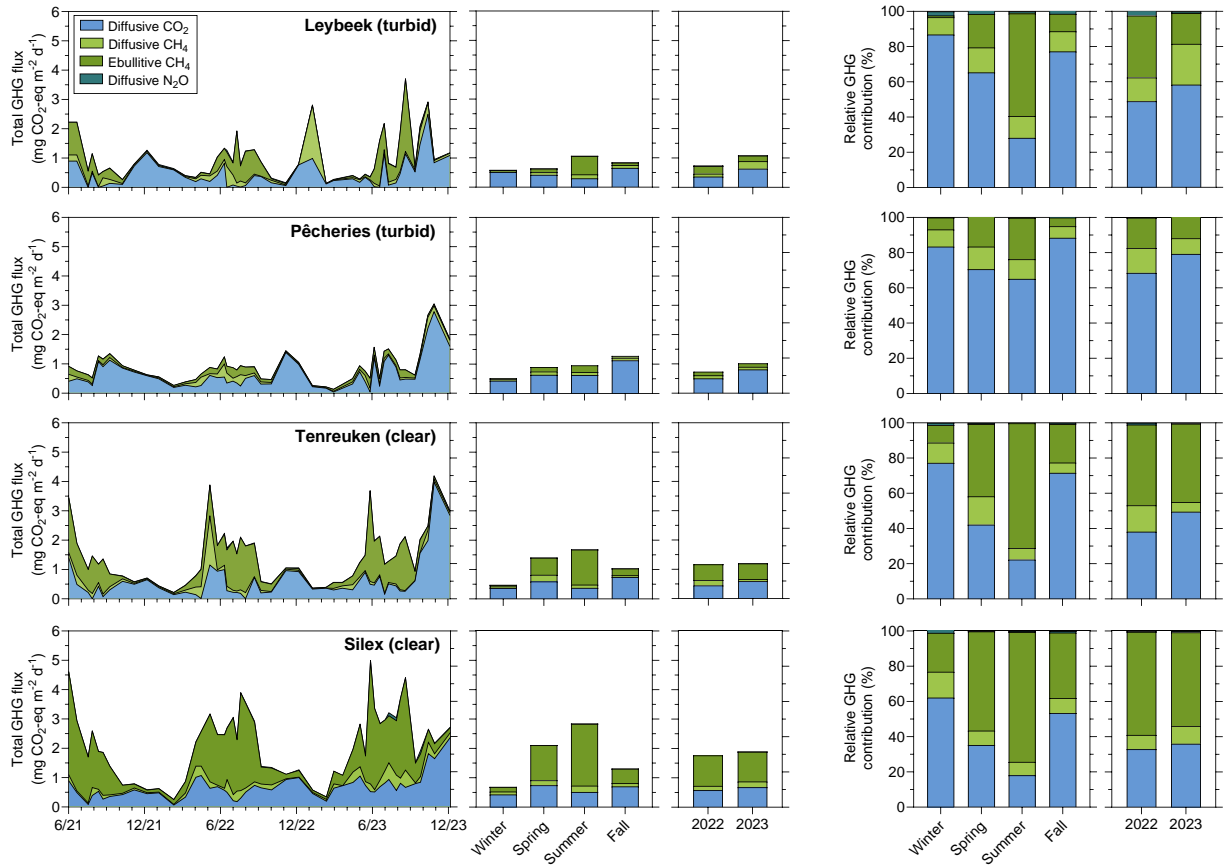
587

588 **Figure 7: Seasonal variations of diffusive and ebullitive CH<sub>4</sub> fluxes (mmol m<sup>-2</sup> d<sup>-1</sup>), and the ratio of ebullitive CH<sub>4</sub> flux to total  
589 (ebullitive+diffusive) CH<sub>4</sub> flux (%) in four urban ponds (Leybeek (Leyb), Pêcheries (Pech), Tenreuken (Trk), and Silex (Slx)) in  
590 the city of Brussels (Belgium) from June 2021 to December 2023. Diffusive fluxes were calculated from CH<sub>4</sub> concentration and gas  
591 transfer velocity derived from wind speed. Ebullitive CH<sub>4</sub> fluxes were calculated from the relations with water temperature for  
592 each pond (Fig. 6; Table S7) from the water temperature data coincident with the diffusive CH<sub>4</sub> fluxes. Box plots show median  
593 (horizontal line), mean (cross), and 25–75% percentiles (box limits). Whiskers extend from minimum to maximum values. White  
594 and grey bands in the graphs on the right correspond with the autumn/winter and spring/summer periods, respectively, and  
595 dotted vertical bars represent the first days of each season. Lower case letters indicate significant differences between ponds  
596 (Tables S3 and S4).**



597

598 **Figure 8: Mean diffusive and ebullitive CH<sub>4</sub> fluxes (mmol m<sup>-2</sup> d<sup>-1</sup>) and mean ratio of ebullitive CH<sub>4</sub> flux to total**  
 599 **(diffusive+ebullitive) CH<sub>4</sub> flux (%) versus chlorophyll-*a* (Chl-*a*, in µg L<sup>-1</sup>), total macrophyte cover in summer (%), water depth**  
 600 **(m), and lake surface area (ha) in four ponds (Leybeek, Pêcheries, Tenreuken, and Silex) in the city of Brussels (Belgium) from**  
 601 **June 2021 to December 2023. Error bars indicate the standard deviation. Solid lines indicate either linear or polynomial fits.**  
 602 **Statistical comparisons between the four ponds are summarized in Table S3.**



603

604 **Figure 9: Temporal evolution and relative contribution of emissions to the atmosphere of  $\text{CO}_2$  (diffusive),  $\text{CH}_4$  (diffusive and**

605 **ebullitive), and  $\text{N}_2\text{O}$  (diffusive) expressed in  $\text{CO}_2$  equivalents (in  $\text{mg CO}_2\text{-eq m}^{-2} \text{d}^{-1}$ ), in four urban ponds (Leybeek, Pêcheries,**

606 **Tenreuken, and Silex) in the city of Brussels (Belgium) from June 2021 to December 2023. Averages per season include data from**

607 **2021, 2022, and 2023. Year 2023 had a higher annual precipitation (1011 mm) than year 2022 (701 mm).**

608 **Data availability.** The full data-set is available at 10.5281/zenodo.11103556.

609 **Author contributions.** AVB and NG conceived the study; TB collected field samples; TB and AVB made the laboratory  
610 analysis; TB and AVB jointly interpreted data and drafted the manuscript with substantial inputs from NG.

611 **Competing interests.** The authors declare that they have no conflict of interest.

612 **Acknowledgements.** We thank Ozan Efe (University of Liège) and Adriana Anzil (Université Libre de Bruxelles) for  
613 analytical assistance, Florence Charlier (Université Libre de Bruxelles) for help in macrophyte identification and density  
614 quantification (Table S1), Bruxelles Environnement for providing information on history of operations in the ponds (Table  
615 S2), two anonymous reviewers and Associate Editor (Gabriel Singer) for comments and suggestions on the initial  
616 manuscript.

617 **Financial support.** TB received funding from the Brussels-Capital Region's institute for the encouragement of scientific  
618 research and innovation (Innoviris) as part of the Smartwater project (RBC/2020-EPF-6 h) and from the "Fonds pour la  
619 formation à la Recherche dans l'Industrie et dans l'Agriculture" (FRIA, Belgium). AVB is a Research Director at the FRS-  
620 FNRS.

621 **References**

622 Aben, R. C. H., Barros, N., Van Donk, E., Frenken, T., Hilt, S., Kazanjian, G., Lamers, L. P. M., Peeters, E. T. H. M.,  
623 Roelofs, J.G.M., de Senerpont Domis, L. S., Stephan, S., Velthuis, M., Van de Waal, D., Wik, M., Thornton, B.,  
624 Wilkinson, J., Delsontro, T., and Kosten, S.: Cross continental increase in methane ebullition under climate change.  
625 *Nature communications*, 8(1), 1682. <https://doi.org/10.1038/s41467-017-01535-y>, 2017.

626 Audet, J., Neif, É.M., Cao, Y., Hoffmann, C.C., Lauridsen, T.L., Larsen, S.E., Søndergaard, M., Jeppesen, E., and Davidson,  
627 T.A.: Heat-wave effects on greenhouse gas emissions from shallow lake mesocosms. *Freshwater  
628 Biology*. 2017; 62: 1130–1142. <https://doi.org/10.1111/fwb.12930>, 2017.

629 Audet, J., Carstensen, M.V., Hoffmann, C.C., Lavaux, L., Thieme, K., and Davidson, T.A.: Greenhouse gas emissions from  
630 urban ponds in Denmark. *Inland Waters*, 10 (3), 373–385. <https://doi.org/10.1080/20442041.2020.1730680>, 2020.

631 Baliña, S., Sanchez, M. L., Izaguirre, I., and del Giorgio, P. A.: Shallow lakes under alternative states differ in the dominant  
632 greenhouse gas emission pathways. *Limnology and Oceanography*, 68(1), 1-13. <https://doi.org/10.1002/lno.12243>,  
633 2023.

634 Barko, J. W., Gunnison, D., and Carpenter, S. R.: Sediment interactions with submersed macrophyte growth and community  
635 dynamics. *Aquatic botany*, 41(1-3), 41-65. [https://doi.org/10.1016/0304-3770\(91\)90038-7](https://doi.org/10.1016/0304-3770(91)90038-7), 1991.

636 Bartosiewicz, M., Maranger, R., Przytulska, A., and Laurion, I.: Effects of phytoplankton blooms on fluxes and emissions of  
637 greenhouse gases in a eutrophic lake. *Water Research*, 196, 116985. <https://doi.org/10.1016/j.watres.2021.116985>,  
638 2021.

639 Bastviken, D., Ejlertsson, J. and Tranvik, L.: Measurement of methane oxidation in lakes: A comparison of methods.  
640 *Environmental Science & Technology*, 36, 3354-3361. <https://doi.org/10.1021/es010311p>, 2002.

641 Bastviken, D., Treat, C.C., Pangala, S.R., Gauci, V., Enrich-Prast, A., Karlson, M., Gålfalk, M., Romano, M.B., and  
642 Sawakuchi, H.O.: The importance of plants for methane emission at the ecosystem scale. *Aquatic Botany*, 184,  
643 103596. <https://doi.org/10.1016/j.aquabot.2022.103596>, 2023.

644 Bates, D., Maechler, M., Bolker, B., and Walker, S.: Fitting linear mixed-effects models using lme4. *Journal of Statistical  
645 Software*, 67, 1–48. <https://doi.org/10.1126/science.1176170>, 2015.

646 Bauduin, T., Gypens, N., and Borges, A.V.: Seasonal and spatial variations of greenhouse gas (CO<sub>2</sub>, CH<sub>4</sub> and N<sub>2</sub>O)  
647 emissions from urban ponds in Brussels. *Water Research*, 121257. <https://doi.org/10.1016/j.watres.2024.121257>,  
648 2024.

649 Borges, A.V., Darchambeau, F., Lambert, T., Morana, C., Allen, G.H., Tambwe, E., and Bouillon, S.: Variations in  
650 dissolved greenhouse gases (CO<sub>2</sub>, CH<sub>4</sub>, N<sub>2</sub>O) in the Congo River network overwhelmingly driven by fluvial-  
651 wetland connectivity. *Biogeosciences*, 16 (19), 3801–3834. <https://doi.org/10.5194/bg-16-3801-2019>, 2019.

652 Borges, A.V., Deirmendjian, L., Bouillon, S., Okello, W., Lambert, T., Roland, F.A.E., Razanamahandry, V.F., Voarintsoa,  
653 N.R.G., Darchambeau, F., Kimirei, I.A., Descy, J., Allen, G.H., and Morana, C.: Greenhouse gas emissions from  
654 African lakes are no longer a blind spot. *Sciences Advances*, 8 (25), eabi8716. <https://doi.org/10.1126/sciadv.abi8716>, 2022.

656 Borges, A.V., Okello, W., Bouillon, S., Deirmendjian, S., Nankabirwa, A., Nabafu, E., Lambert, T., Descy, J-P, and Morana,  
657 C.: Spatial and temporal variations of dissolved CO<sub>2</sub>, CH<sub>4</sub> and N<sub>2</sub>O in Lakes Edward and George (East Africa).  
658 *Journal of Great Lakes Research*, 49, 229-245, <https://doi.org/10.1016/j.jglr.2022.11.010>, 2023.

659 Brans, K.I., Engelen, J.M., Souffreau, C., and De Meester, L.: Urban hot-tubs: local urbanization has profound effects on  
660 average and extreme temperatures in ponds. *Landscape and Urban Planning*, 176, 22–29. <https://doi.org/10.1016/j.lup.2018.07.018>.

662 Cael, B. B., Heathcote, A. J., and Seekell, D. A.: The volume and mean depth of Earth's lakes. *Geophysical Research  
663 Letters*, 44(1), 209-218. <https://doi.org/10.1002/2016GL071378>, 2017.

664 Casas-Ruiz, J.P., Jakobsson, J., and del Giorgio, P.A.: The role of lake morphometry in modulating surface water carbon  
665 concentrations in boreal lakes. *Environmental Research Letters*, 16 (7), 074037 <https://doi.org/10.1088/1748-9326/ac0be3>, 2021.

667 Chen, B., Zhang, L., and Wang, C.: Distinct impacts of the central and eastern Atlantic Niño on the European climate.  
668 *Geophysical Research Letters*, 51(2), e2023GL107012. <https://doi.org/10.1029/2023GL107012>, 2024.

669 Choudhury, M. I., McKie, B. G., Hallin, S., and Ecke, F.: Mixtures of macrophyte growth forms promote nitrogen cycling in  
670 wetlands. *Science of the Total Environment*, 635, 1436-1443. <https://doi.org/10.1016/j.scitotenv.2018.04.193>, 2018.

671 Clifford, C.C., and Heffernan, J.B.: Artificial aquatic ecosystems. *Water*, 10 (8), 1096. <https://doi.org/10.3390/w10081096>,  
672 2018.

673 Codispoti, L.A., and Christensen, J.P.: Nitrification, denitrification and nitrous oxide cycling in the eastern tropical South  
674 Pacific Ocean. *Marine chemistry*, 16 (4), 277–300. [https://doi.org/10.1016/0304-4203\(85\)90051-9](https://doi.org/10.1016/0304-4203(85)90051-9), 1985.

675 Cole, J.J., and Caraco, N.F.: Atmospheric exchange of carbon dioxide in a low-wind oligotrophic lake measured by the  
676 addition of SF<sub>6</sub>. *Limnology and Oceanography*, 43 (4), 647–656. <https://doi.org/10.4319/lo.1998.43.4.0647>, 1998.

677 Dan, Z., Chuan, W., Qiaohong, Z., and Xingzhong, Y.: Sediments nitrogen cycling influenced by submerged macrophytes  
678 growing in winter. *Water Science and Technology*, 83(7), 1728-1738. <https://doi.org/10.2166/wst.2021.081>, 2021.

679 Davidson, T.A., Audet, J., Svenning, J.C., Lauridsen, T.L., Søndergaard, M., Landkildehus, F., and Jeppesen, E.:  
680 Eutrophication effects on greenhouse gas fluxes from shallow-lake mesocosms override those of climate warming.  
681 *Global Change Biology*, 21 (12), 4449–4463. <https://doi.org/10.1111/gcb.13062>, 2015.

682 Deemer, B. R., and Holgerson, M. A.: Drivers of methane flux differ between lakes and reservoirs, complicating global  
683 upscaling efforts. *Journal of Geophysical Research: Biogeosciences*, 126(4) <https://doi.org/10.1029/2019JG005600>  
684 , 2021.

685 DelSontro, T., Beaulieu, J. J., and Downing, J. A.: Greenhouse gas emissions from lakes and impoundments: Upscaling in  
686 the face of global change. *Limnology and Oceanography Letters*, 3(3), 64-75. <https://doi.org/10.1002/lol2.10073>,  
687 2018.

688 DelSontro, T., Kunz, M. J., Kempfer, T., Wüest, A., Wehrli, B., and Senn, D. B.: Spatial Heterogeneity of Methane  
689 Ebullition in a Large Tropical Reservoir, *Environmental Science & Technology*, 45 (23), 9866-9873,  
690 <https://doi.org/10.1021/es2005545>, 2011.

691 DelSontro, T., Boutet, L., St-Pierre, A., del Giorgio, P.A., and Prairie, Y.T.: Methane ebullition and diffusion from northern  
692 ponds and lakes regulated by the interaction between temperature and system productivity, *Limnology and*  
693 *Oceanography*, 61(S1), S62-S77 <https://doi.org/10.1002/lno.10335>, 2016.

694 Deng, Hg., Zhang, J., Wu, J., Yao, X., and Yang, L.-W.: Biological denitrification in a macrophytic lake: implications for  
695 macrophytes-dominated lake management in the north of China. *Environmental Sciences and Pollution Research*,  
696 27, 42460–42471. <https://doi.org/10.1007/s11356-020-10230-3>, 2020.

697 Desrosiers, K., DelSontro, T., and del Giorgio, P.A.: Disproportionate Contribution of Vegetated Habitats to the CH<sub>4</sub> and  
698 CO<sub>2</sub> Budgets of a Boreal Lake. *Ecosystems*, 1-20. <https://doi.org/10.1007/s10021-021-00730-9>, 2022.

699 Dickson, A.G.; Sabine, C.L. and Christian, J.R.: Guide to best practices for ocean CO<sub>2</sub> measurement. Sidney, British  
700 Columbia, North Pacific Marine Science Organization, 191pp. (PICES Special Publication 3; IOCCP Report 8).  
701 <https://doi.org/10.25607/OPB-1342>, 2007.

702 Dutton, G., Elkins II, J., Hall, B., NOAA ESRL, Earth System Research Laboratory Halocarbons and Other Atmospheric  
703 Trace Gases Chromatograph for Atmospheric Trace Species (CATS) Measurements. NOAA National Centers for  
704 Environmental Information. <https://doi.org/10.7289/V5X0659V>. Version 1. [Database: atmospheric nitrous oxide  
705 N<sub>2</sub>O] [2024-03-27], 2023.

706 Goeckner, A. H., Lusk, M. G., Reisinger, A. J., Hosen, J. D., and Smoak, J. M.: Florida's urban stormwater ponds are net  
707 sources of carbon to the atmosphere despite increased carbon burial over time. *Communications earth &*  
708 *environment*, 3(1), 53, <https://doi.org/10.1038/s43247-022-00384-y> 2022.

709 Gorsky, A. L., Dugan, H. A., Wilkinson, G. M., and Stanley, E. H.: Under-ice oxygen depletion and greenhouse gas  
710 supersaturation in north temperate urban ponds. *Journal of Geophysical Research: Biogeosciences*, 129(6),  
711 <https://doi.org/10.1029/2024JG008120>, 2024.

712 Gorsky, A.L., Racanelli, G.A., Belvin, A.C., and Chambers, R.M.: Greenhouse gas flux from stormwater ponds in  
713 southeastern Virginia (USA). *Anthropocene*, 28, 100218. <https://doi.org/10.1016/j.ancene.2019.100218>, 2019.

714 Grasset, C., Abril, G., Mendonça, R., Roland, F., and Sobek, S.: The transformation of macrophyte-derived organic matter to  
715 methane relates to plant water and nutrient contents. *Limnology and Oceanography*, 64(4), 1737-1749,  
716 <https://doi.org/10.1002/lno.11148>, 2019.

717 Grasset, C., Sobek, S., Scharnweber, K., Moras, S., Villwock, H., Andersson, S., Hiller, C., Nydahl, A.C., Chaguaceda, F.,  
718 Colom, W., and Tranvik, L.J.: The CO<sub>2</sub>-equivalent balance of freshwater ecosystems is non-linearly related to  
719 productivity. *Global Change Biology*, 26 (10), 5705–5715. <https://doi.org/10.1111/gcb.15284>, 2020.

720 Grasshoff, K., and Johannsen, H.: A new sensitive and direct method for the automatic determination of ammonia in sea  
721 water. *ICES Journal of Marine Science*, 34 (3), 516–521. <https://doi.org/10.1093/icesjms/34.3.516>, 1972.

722 Grasshoff, K., Kremling, K., and Ehrhardt, M.: Methods of Seawater Analysis: Determination of Nitrite. John Wiley & Sons,  
723 2009.

724 Grinham, A., Albert, S., Deering, N., Dunbabin, M., Bastviken, D., Sherman, B., Lovelock, C.E., and Evans, C.D.: The  
725 importance of small artificial water bodies as sources of methane emissions in Queensland, Australia. *Hydrology*  
726 and *Earth System Sciences*, 22 (10), 5281–5298. <https://doi.org/10.5194/hess-22-5281-2018>, 2018.

727 Harpenslager, S. F., Thieme, K., Levertz, C., Misteli, B., Sebola, K. M., Schneider, S. C., Hilt, S., and Köhler, J.: Short-term  
728 effects of macrophyte removal on emission of CO<sub>2</sub> and CH<sub>4</sub> in shallow lakes. *Aquatic Botany*, 182, 103555.  
729 <https://doi.org/10.1016/j.aquabot.2022.103555>, 2022.

730 Hassall, C., The ecology and biodiversity of urban ponds. *WIREs Water*, 1: 187-206. <https://doi.org/10.1002/wat2.1014>,  
731 2014.

732 Herrero Ortega, S., Romero González-Quijano, C., Casper, P., Singer, G.A., and Gessner, M.O.: Methane emissions from  
733 contrasting urban freshwaters: rates, drivers, and a whole-city footprint. *Global change biology*, 25 (12), 4234–  
734 4243. <https://doi.org/10.1111/gcb.14799>, 2019.

735 Hilt, S., Brothers, S., Jeppesen, E., Veraart, A. J., and Kosten, S.: Translating regime shifts in shallow lakes into changes in  
736 ecosystem functions and services. *BioScience*, 67(10), 928–936. <https://doi.org/10.1093/biosci/bix106>, 2017.

737 Holgerson, M., and Raymond, P.: Large contribution to inland water CO<sub>2</sub> and CH<sub>4</sub> emissions from very small ponds. *Nature  
738 Geoscience*, 9, 222–226. <https://doi.org/10.1038/ngeo2654>, 2016.

739 Holgerson, M.A.: Drivers of carbon dioxide and methane supersaturation in small, temporary ponds, *Biogeochemistry*, 124,  
740 305–318. <https://doi.org/10.1007/s10533-015-0099-y>, 2015.

741 Huttunen, J. T., Alm, J., Liikanen, A., Juutinen, S., Larmola, T., Hammar, T., Silvola, T., and Martikainen, P. J.: Fluxes of  
742 methane, carbon dioxide and nitrous oxide in boreal lakes and potential anthropogenic effects on the aquatic  
743 greenhouse gas emissions. *Chemosphere*, 52(3), 609–621. [https://doi.org/10.1016/S0045-6535\(03\)00243-1](https://doi.org/10.1016/S0045-6535(03)00243-1), 2003.

744 Hyvönen, T., Ojala, A., Kankaala, P., & Martikainen, P. J.: Methane release from stands of water horsetail (*Equisetum  
745 fluviatile*) in a boreal lake, *Freshwater Biology*, 40, 275– 284. <https://doi.org/10.1046/j.1365-2427.1998.00351.x>,  
746 1998.

747 Johnson, M.S., Matthews, E., Du, J., Genovese, V., and Bastviken, D.: Methane Emission from Global Lakes: New  
748 Spatiotemporal Data and Observation-Driven Modeling of Methane Dynamics Indicates Lower Emissions. *Journal  
749 of Geophysical Research: Biogeosciences*, 127(7). <https://doi.org/10.1029/2022JG006793>, 2022.

750 Juutinen, S., Alm, J., Larmola, T., Huttunen, J. T., Morero, M., Martikainen, P. J., and Silvola, J.: Major implication of the  
751 littoral zone for methane release from boreal lakes, *Global biogeochemical cycles*, 17(4), 1117,  
752 <https://doi.org/10.1029/2003GB002105>, 2003.

753 Kankaala, P., Huotari, J., Tulonen, T., and Ojala, A.: A Lake-size dependent physical forcing drives carbon dioxide and  
754 methane effluxes from lakes in a boreal landscape. *Limnology and Oceanography*, 58:1915–1930.  
755 <https://doi.org/10.4319/lo.2013.58.6.1915>, 2013.

756 Keller, M., and Stallard, R. F.: Methane emission by bubbling from Gatun Lake, Panama, *Journal of Geophysical Research:  
757 Atmospheres*, 99(D4), 8307–8319, doi:10.1029/92JD02170, 1994.

758 Koroleff, J.: Determination of total phosphorus by alkaline persulphate oxidation. *Methods of Seawater Analysis*. Verlag  
759 Chemie, Wienheim, pp. 136–138, 1983.

760 Kosten, S., Roland, F., Da Motta Marques, D. M., Van Nes, E. H., Mazzeo, N., Sternberg, L. D. S., Scheffer, M., and Cole,  
761 J. J. Climate-dependent CO<sub>2</sub> emissions from lakes. *Global Biogeochemical Cycles*, 24(2).  
762 <https://doi.org/10.1029/2009GB003618>, 2010.

763 Lan, X., K.W. Thoning, and E.J. Dlugokencky: Trends in globally-averaged CH<sub>4</sub>, N<sub>2</sub>O, and SF<sub>6</sub> determined from NOAA  
764 Global Monitoring Laboratory measurements [data set]. Version 2024-08, <https://doi.org/10.15138/P8XG-AA10>,  
765 2024.

766 Lauerwald, R., Regnier, P., Figueiredo, V., Enrich-Prast, A., Bastviken, D., Lehner, B., Maavara, T., and Raymond, P.:  
767 Natural Lakes Are a Minor Global Source of N<sub>2</sub>O to the Atmosphere. *Global Biogeochemical Cycles*, 33(12),  
768 1564–1581. <https://doi.org/10.1029/2019GB006261>, 2019.

769 Lauerwald, R., Allen, G. H., Deemer, B. R., Liu, S., Maavara, T., Raymond, P., Alcott, L., Bastviken, D., Hastie, A.,  
770 Holgerson, M.A., Johnson, M. S., Lehner, B., Lin, P., Marzadri, A., Ran, L., Tian, H., Yang, X., Yao, Y., and  
771 Regnier, P.: Inland water greenhouse gas budgets for RECCAP2: 2. Regionalization and homogenization of  
772 estimates. *Global Biogeochemical Cycles*, 37, e2022GB007658. <https://doi.org/10.1029/2022GB007658>, 2023.

773 Liu, W., Jiang, X., Zhang, Q., Li, F., and Liu, G.: Has submerged vegetation loss altered sediment denitrification, N<sub>2</sub>O  
774 production, and denitrifying microbial communities in subtropical lakes? *Global Biogeochemical Cycles*, 32, 1195–  
775 1207. <https://doi.org/10.1029/2018GB005978>, 2018.

776 Maavara, T., Lauerwald, R., Laruelle, G. G., Akbarzadeh, Z., Bouskill, N. J., Van Cappellen, P., and Regnier, P.: Nitrous  
777 oxide emissions from inland waters: Are IPCC estimates too high? *Global Change Biology*, 25(2), 473–488.  
778 <https://doi.org/10.1111/gcb.145042>, 2019.

779 Marotta, H., Duarte, C. M., Pinho, L., and Enrich-Prast, A.: Rainfall leads to increased pCO<sub>2</sub> in Brazilian coastal lakes.  
780 *Biogeosciences*, 7(5), 1607-1614. <https://doi.org/10.5194/bg-7-1607-2010>, 2010.

781 Martinez-Cruz, K., Gonzalez-Valencia, R., Sepulveda-Jauregui, A., Plascencia- Hernandez, F., Belmonte-Izquierdo, Y., and  
782 Thalasso, F.: Methane emission from aquatic ecosystems of Mexico City. *Aquatic Sciences*, 79, 159–169.  
783 <https://doi.org/10.1007/s00027-016-0487-y>, 2017.

784 Mengis, M., Gächter, R., and Wehrli, B.: Sources and sinks of nitrous oxide (N<sub>2</sub>O) in deep lakes. *Biogeochemistry*, 38, 281-  
785 301. <https://doi.org/10.1023/A:1005814020322>, 1997.

786 Myrhe, G., Shindell, D., Bréon, F.M., Collins, W., and Al, E. Anthropogenic and natural radiative forcing. Climate Change  
787 2013 the Physical Science Basis: working Group I Contribution to the Fifth Assessment Report of the  
788 Intergovernmental Panel on Climate Change. Chapter 8 : Anthropogenic and Natural Radiative Forcing  
789 9781107057, 659–740. <https://doi.org/10.1017/CBO9781107415324.018>, 2013.

790 Natchimuthu, S., Panneer Selvam, B., and Bastviken, D.: Influence of weather variables on methane and carbon dioxide flux  
791 from a shallow pond. *Biogeochemistry*, 119, 403–413. <https://doi.org/10.1007/s10533-014-9976-z>, 2014.

792 Natchimuthu, S., Sundgren, I., Gålfalk, M., Klemmedsson, L., Crill, P., Danielsson, Å. and Bastviken, D. (2016), Spatio-  
793 temporal variability of lake CH<sub>4</sub> fluxes and its influence on annual whole lake emission estimates. *Limnology and*  
794 *Oceanography*, 61: S13-S26. <https://doi.org/10.1002/lno.10222>, 2016.

795 Ni, M., Liang, X., Hou, L., Li, W., and He, C.: Submerged macrophytes regulate diurnal nitrous oxide emissions from a  
796 shallow eutrophic lake: A case study of Lake Wuliangsu in the temperate arid region of China. *Science of The*  
797 *Total Environment*, 811, 152451. <https://doi.org/10.1016/j.scitotenv.2021.152451>, 2022.

798 Ojala A., Bellido J.L., Tulonen T., Kankaala P., and Huotari J.: Carbon gas fluxes from a brown-water and a clear-water lake  
799 in the boreal zone during a summer with extreme rain events, *Limnology and Oceanography*, 56,  
800 <https://doi.org/10.4319/lo.2011.56.1.0061>, 2011.

801 Ollivier, Q.R., Maher, D.T., Pitfield, C., and Macreadie, P.I.: Punching above their weight: large release of greenhouse gases  
802 from small agricultural dams. *Global change biology*, 25 (2), 721–732. <https://doi.org/10.1111/gcb.14477>, 2019.

803 Peacock, M., Audet, J., Bastviken, D., Cook, S., Evans, C.D., Grinham, A., Holgerson, M. A., Högbom, L., Pickard, A.E.,  
804 Zieliński, P., and Futter, M.N.: Small artificial waterbodies are widespread and persistent emitters of methane and  
805 carbon dioxide. *Global change biology*, 27 (20), 5109–5123. <https://doi.org/10.1111/gcb.15762>, 2021.

806 Peacock, M., Audet, J., Jordan, S., Smeds, J., and Wallin, M.B.: Greenhouse gas emissions from urban ponds are driven by  
807 nutrient status and hydrology. *Ecosphere*, 10 (3), e02643. <https://doi.org/10.1002/ecs2.2643>, 2019.

808 Peretyatko, A., Symoens, J. J., and Triest, L.: Impact of macrophytes on phytoplankton in eutrophic peri-urban ponds,  
809 implications for pond management and restoration. *Belgian Journal of Botany*, 83-99.  
810 <https://doi.org/10.2307/20794626>, 2007.

811 R Core Team (2021). R: A language and environment for statistical computing. R Foundation for Statistical Computing,  
812 Vienna, Austriaa. <https://www.R-project.org/>, 2021.

813 Rabaey, J. and Cotner, J.: Pond greenhouse gas emissions controlled by duckweed coverage. *Frontiers in environmental*  
814 *science*, 10, 889289 <https://doi.org/10.3389/fenvs2022.889289>, 2022.

815 Rabaey, J. and Cotner, J.: The influence of mixing on seasonal carbon dioxide and methane fluxes in ponds.  
816 *Biogeochemistry*, 1-18, <https://doi.org/10.1007/s10533-024-01167-7>, 2024.

817 Rasilo, T., Ojala, A., Huotari, J. and Pumpanen, J.: Rain Induced Changes in Carbon Dioxide Concentrations in the Soil-  
818 Lake-Brook Continuum of a Boreal Forested Catchment. *Vadose Zone Journal*, 11: vzh2011.0039.  
819 <https://doi.org/10.2136/vzh2011.0039>, 2012.

820 Ray, N. E., and Holgerson, M. A.: High Intra-Seasonal Variability in Greenhouse Gas Emissions from Temperate  
821 Constructed Ponds. *Geophysical Research Letters*, 50(18), e2023GL104235,  
822 <https://doi.org/10.1029/2023GL104235>, 2023.

823 Ray, N. E., Holgerson, M. A., Andersen, M. R., Bikše, J., Bortolotti, L. E., Futter, M., Kokorite, I., Law, A., McDonald, C.,  
824 Mesman, J.P., Peacock, M., Richardson, D.C., Arsenault, J., Bansal, S., Cawley, K., Kuhn, M., Shahabinia, A.R.,  
825 and Smufer, F.: Spatial and temporal variability in summertime dissolved carbon dioxide and methane in  
826 temperate ponds and shallow lakes. *Limnology and Oceanography*, 68(7), 1530-1545.  
827 <https://doi.org/10.1002/lno.12362>, 2023.

828 Raymond, P. A., Hartmann, J., Lauerwald, R., Sobek, S., McDonald, C., Hoover, M., Butman, D., Striegl, R., Mayorga, E.,  
829 Humborg, C., Kortelainen, P., Dürr, H., Meybeck, M., Ciais, P., and Guth, P.: Global carbon dioxide emissions  
830 from inland waters. *Nature*, 503(7476), 355–359. <https://doi.org/10.1038/nature12760>, 2013.

831 Reitsema, R. E., Meire, P., and Schoelynck, J.: The future of freshwater macrophytes in a changing world: dissolved organic  
832 carbon quantity and quality and its interactions with macrophytes. *Frontiers in Plant Science*, 9, 301954.  
833 <https://doi.org/10.3389/fpls.2018.00629>, 2018.

834 Rocher-Ros, G., Stanley, E. H., Loken, L. C., Casson, N. J., Raymond, P. A., Liu, S., Amatulli, G., and Sponseller, R. A.:  
835 Global methane emissions from rivers and streams. *Nature*, 621:530–535. <https://doi.org/10.1038/s41586-023-06344-6>, 2023.

837 Rosentreter, J. A., Borges, A. V., Deemer, B. R., Holgerson, M. A., Liu, S., Song, C., Melack, J., Raymond, P. A., Duarte, C.  
838 M., Allen, G. H., Olefeldt, D., Poulter, B., Battin, T. I., and Eyre, B. D.: Half of global methane emissions come  
839 from highly variable aquatic ecosystem sources. *Nature Geoscience*, 14(4), 225–230.  
840 <https://doi.org/10.1038/s41561-021-00715-2>, 2021.

841 Sand-Jensen, K., & Staehr, P. A.: Scaling of pelagic metabolism to size, trophy and forest cover in small Danish lakes.  
842 *Ecosystems*, 10, 128-142. <https://doi.org/10.1007/s10021-006-9001-z>, 2007.

843 Scandella, B. P., Varadharajan, C., Hemond, H. F., Ruppel, C., and Juanes, R.: A conduit dilation model of methane venting  
844 from lake sediments. *Geophysical Research Letters*, 38(6). <https://doi.org/10.1029/2011GL046768>, 2011.

845 Scheffer, M., Hosper, S. H., Meijer, M. L., Moss, B., and Jeppesen, E.: Alternative equilibria in shallow lakes. *Trends in  
846 ecology & evolution*, 8(8), 275-279. [https://doi.org/10.1016/0169-5347\(93\)90254-M](https://doi.org/10.1016/0169-5347(93)90254-M), 1993.

847 Schulz, S. and Conrad, R.: Influence of temperature on pathways to methane production in the permanently cold profundal  
848 sediment of Lake Constance. *FEMS Microbiology Ecology*, 20 1-14; <https://doi.org/10.1111/j.1574-6941.1996.tb00299.x>, 1996.

850 Singh, S.N., Kulshreshtha, K., and Agnihotri, S.: Seasonal dynamics of methane emission from wetlands. *Chemosphere-  
851 Global Change Science*, 2 (1), 39–46. [https://doi.org/10.1016/S1465-9972\(99\)00046-X](https://doi.org/10.1016/S1465-9972(99)00046-X), 2000.

852 Stanley, E. H., Casson, N. J., Christel, S. T., Crawford, J. T., Loken, L. C., and Oliver, S. K.: The ecology of methane in  
853 streams and rivers: patterns, controls, and global significance. *Ecological Monographs*, 86(2), 146–171.  
854 <https://doi.org/10.1890/15-1027>, 2016.

855 Taoka, T., Iwata, H., Hirata, R., Takahashi, Y., Miyabara, Y., and Itoh, M.: Environmental controls of diffusive and  
856 ebullitive methane emissions at a subdaily time scale in the littoral zone of a midlatitude shallow lake. *Journal of  
857 Geophysical Research: Biogeosciences*, 125, e2020JG005753. <https://doi.org/10.1029/2020JG005753>, 2020.

858 Theus, M. E., Ray, N. E., Bansal, S., and Holgerson, M. A.: Submersed macrophyte density regulates aquatic greenhouse gas  
859 emissions. *Journal of Geophysical Research: Biogeosciences*, 128(10), <https://doi.org/10.1029/2023JG007758>,  
860 2023.

861 Tixier, G., M Lafont, M., L Grapentine, L., Q Rochfort, Q., and J Marsalek, J.: Ecological risk assessment of urban  
862 stormwater ponds: Literature review and proposal of a new conceptual approach providing ecological quality goals  
863 and the associated bioassessment tools, *Ecological Indicators*, 11, 1497-1506,  
864 <https://doi.org/10.1016/j.ecolind.2011.03.027>, 2011.

865 Tokida, T., Miyazaki, T., Mizoguchi, M., Nagata, O., Takakai, F., Kagemoto, A., and Hatano, R.: Falling atmospheric  
866 pressure as a trigger for methane ebullition from peatland. *Global Biogeochemical Cycles*, 21(2).  
867 <https://doi.org/10.1029/2006GB002790>, 2007.

868 Vachon, D., and del Giorgio, P.A. Whole-Lake CO<sub>2</sub> Dynamics in Response to Storm Events in Two Morphologically  
869 Different Lakes. *Ecosystems*, 17, 1338–1353 (2014). <https://doi.org/10.1007/s10021-014-9799-8>, 2014.

870 Vachon, D., Langenegger, T., Donis, D., Beaubien, S. E., and McGinnis, D. F.: Methane emission offsets carbon dioxide  
871 uptake in a small productive lake. *Limnology and Oceanography Letters*, 5(6), 384–392,  
872 <https://doi.org/10.1002/lol2.10161>, 2020.

873 van Bergen, T.J.H.M., Barros, N., Mendonça, R., Aben, R.C.H., Althuizen, I.H.J., Huszar, V., Lamers, L.P.M., Lürling, M.,  
874 Roland, F., and Kosten, S.: Seasonal and diel variation in greenhouse gas emissions from an urban pond and its  
875 major drivers. *Limnology and Oceanography*, 64 (5), 2129–2139. <https://doi.org/10.1002/1no.11173>, 2019.

876 Varadharajan, C., and Hemond, H. F.: Time - series analysis of high - resolution ebullition fluxes from a stratified,  
877 freshwater lake. *Journal of Geophysical Research: Biogeosciences*, 117(G2).  
878 <https://doi.org/10.1029/2011JG001866>, 2012.

879 Velthuis, M., and Veraart, A. J.: Temperature sensitivity of freshwater denitrification and N<sub>2</sub>O emission—A meta-analysis.  
880 *Global Biogeochemical Cycles*, 36(6), <https://doi.org/10.1029/2022GB007339>, 2022.

881 Verpoorter, C., Kutser, T., Seekell, D. A., and Tranvik, L. J.: A global inventory of lakes based on high - resolution satellite  
882 imagery. *Geophysical Research Letters*, 41(18), 6396–6402. <https://doi.org/10.1002/2014GL060641>, 2014.

883 Wang, G., Xia, X., Liu, S., Zhang, S., Yan, W., McDowell, W.H.: Distinctive Patterns and Controls of Nitrous Oxide  
884 Concentrations and Fluxes from Urban Inland Waters, *Environmental Science & Technology*, 55, 8422–8431,  
885 <https://doi.org/10.1021/acs.est.1c00647>, 2021.

886 Wanninkhof, R.: Relationship between gas exchange and wind speed over the ocean. *Journal of Geophysical Research: Oceans*, 97, 7373–7381. <https://doi.org/10.1029/92JC00188>, 1992.

888 Webb, J.R., Clough, T.J., Quayle, W.C.: A review of indirect N<sub>2</sub>O emission factors from artificial agricultural waters,  
889 *Environmental Research Letters*, 16 043005, <https://doi.org/10.1088/1748-9326/abed00>, 2021.

890 Webb, J.R., Leavitt, P.R., Simpson, G.L., Baulch, H.M., Haig, H.A., Hodder, K.R., and Finlay, K.: Regulation of carbon  
891 dioxide and methane in small agricultural reservoirs: optimizing potential for greenhouse gas uptake.  
892 *Biogeosciences*, 16 (21), 4211–4227. <https://doi.org/10.5194/bg-16-4211-2019>, 2019.

893 Webb, J.R., Quayle, W.C., Ballester, C., Wells, N.: Semi-arid irrigation farm dams are a small source of greenhouse gas  
894 emissions. *Biogeochemistry*, 166, 123–138. <https://doi.org/10.1007/s10533-023-01100-4>, 2023.

895 Weiss, R. F., Price, B. A.: Nitrous oxide solubility in water and seawater. *Marine chemistry*, 8(4), 347–359.,  
896 [doi.org/10.1016/0304-4203\(80\)90024-9](https://doi.org/10.1016/0304-4203(80)90024-9), 1980.

897 Weiss, R. F.: Determinations of carbon dioxide and methane by dual catalyst flame ionization chromatography and nitrous  
898 oxide by electron capture chromatography. *Journal of Chromatographic Science*, 19, 611–616.  
899 <https://doi.org/10.1093/chromsci/19.12.611>, 1981.

900 West, W.E., Coloso, J.J., and Jones, S.E.: Effects of algal and terrestrial carbon on methane production rates and methanogen  
901 community structure in a temperate lake sediment. *Freshwater Biology*, 57, 949–955.  
902 <https://doi.org/10.1111/j.1365-2427.2012.02755.x>, 2012.

903 Wik, M., Crill, P. M., Varner, R. K., and Bastviken, D.: Multiyear measurements of ebullitive methane flux from three  
904 subarctic lakes. *Journal of Geophysical Research: Biogeosciences*, 118:791 1307–1321.  
905 <https://doi.org/10.1002/jgrg.20103>, 2013.

906 Xie, S., T Xia, T., H Li, H., Y Chen, Y., W Zhang, W. , 2024, Variability in N<sub>2</sub>O emission controls among different ponds  
907 within a hilly watershed, *Water Research*, 267, 122467, <https://doi.org/10.1016/j.watres.2024.122467>, 2024.

908 Xun, F., Feng, M., Ma, S., Chen, H., Zhang, W., Mao, Z., Zhou, Y., Xiao, Q., Wu, Q. L., and Xing, P.: Methane ebullition  
909 fluxes and temperature sensitivity in a shallow lake. *Science of The Total Environment*, 912, 169589.  
910 <https://doi.org/10.1016/j.scitotenv.2023.169589>, 2024.

911 Yan, X., Xu, X., Ji, M., Zhang, Z., Wang, M., Wu, S., Wang, G., Zhang, C., and Liu, H.: Cyanobacteria blooms: A neglected  
912 facilitator of CH<sub>4</sub> production in eutrophic lakes. *Science of the total environment*, 651, 466-474.  
913 <https://doi.org/10.1016/j.scitotenv.2018.09.197>, 2019.

914 Yang, Z., Zhao, Y., and Xia, X.: Nitrous oxide emissions from Phragmites australis-dominated zones in a shallow lake.  
915 *Environmental pollution*, 166, 116-124. <https://doi.org/10.1016/j.envpol.2012.03.006>, 2012.

916 Yentsch, C.S., and Menzel, D.W.: A method for the determination of phytoplankton chlorophyll and phaeophytin by  
917 fluorescence. *Deep Sea Research and Oceanographic Abstracts*, 10. Elsevier, pp. 221-231.  
918 [https://doi.org/10.1016/0011-7471\(63\)90358-9](https://doi.org/10.1016/0011-7471(63)90358-9), 1963.

919 Zhao, K., Tedford, E.W., Zare, M., and Lawrence, G.A.: Impact of atmospheric pressure variations on methane ebullition  
920 and lake turbidity during ice - cover. *Limnology and Oceanography Letters*, 6(5), 253-261.  
921 <https://doi.org/10.1002/lo2.10201>, 2021.

922